

The vast majority of commercial polyolefins are semi-crystalline materials. Depending on the chemical composition and tacticity, their melting temperatures range from ambient to temperatures exceeding 160 °C. Polyolefins form various crystalline structures that can be investigated with microscopic, spectroscopic and scattering techniques.

When a semi-crystalline polyolefin is dissolved in a solvent at high temperature (usually above the melting temperature), followed by a continuous or stepwise decrease of the solution temperature, the polyolefin starts to form crystals that will precipitate out of the solution. The crystallization temperature, the shape and the amount of crystals depend on the molecular structure of the polyolefin, mainly its chemical composition, its tacticity and the degree of branching. Highly crystalline materials will crystallize out of the solution at higher temperatures than materials with lower crystallinity.

Flory–Huggins statistical thermodynamic treatment accounts for melting point depression due to the presence of a diluent in a crystallizing system. The diluent can be a solvent or a comonomer. In either case, the crystallization temperature decreases with increasing diluent concentration. Therefore, for copolymers that do not have long chain branches, the separation by crystallizability can be regarded as a separation according to chemical composition. A precondition is that the concentration of the diluent is low and it does not enter into the crystal lattice of the crystallizing polymer. For copolymers where the non-crystallizing comonomer is the diluent, a linear dependence of the melting or crystallization temperature on the amount of comonomer incorporated is observed. Such linear dependencies have been seen in temperature rising elution fractionation (TREF), differential scanning calorimetry (DSC) and crystallization analysis fractionation (CRYSTAF) experiments [1–4].

The potential of crystallization behaviour of semi-crystalline polymers as an analytical tool was recognized by Desreux and Spiegels [5] in the early history of polyolefin fractionation. TREF, CRYSTAF and crystallization elution fractionation (CEF) are the main techniques that are used today in this category. The differences

in crystallization behaviours of different polymers are the basis of fractionation in these techniques expressed by differences in crystallizability as a function of temperature. A discussion of the various experimental approaches to obtain final results will be given in the following chapters. Long analysis times and the limitation of the techniques to only the crystallizable part of the sample are the major disadvantages of the techniques in this category. The amorphous part cannot be fractionated and is obtained as a bulk fraction. Historically, TREF analysis required around 100 h to be completed. New developments in the field have reduced TREF analysis time to 3–4 h. CRYSTAF analysis can be accomplished in 100 min while the latest development in crystallization-based techniques—CEF—allows analysis to be completed in less than 30 min.

2.1 Temperature Rising Elution Fractionation

There are numerous excellent reviews on TREF that have been published over the years. These reviews demonstrate very clearly that, to date, TREF is the most important fractionation technique for semi-crystalline polyolefins and is a standard method in the polyolefin industry. Most recent and comprehensive reviews have been presented by Soares and Hamielec [6, 7], Monrabal [8, 9] and Pasch, Malik and Macko [10].

The principles of polymer fractionation by solubility or crystallization such as TREF are based on the Flory–Huggins statistical thermodynamic theory that accounts for melting point depression due to the presence of a diluent and it is expressed by Eq. (2.1) [11–14]:

$$1/T_m - 1/T_m^0 = -(R/\Delta H_u) \ln N_A \quad (2.1)$$

where T_m^0 is the melting temperature of the pure polymer, T_m is the equilibrium melting temperature of the ‘diluted’ polymer, ΔH_u is the heat of fusion per polymer repeat unit, and N_A is the mole fraction of the diluent.

Fractionation in TREF resembles a liquid chromatographic separation, comprised of a column, a mobile phase, a set of detectors and a fraction collector. TREF can be performed on analytical and preparative scale, termed A-TREF and P-TREF, respectively. In all cases, a TREF experiment involves the following steps: (1) dissolution of the sample in a suitable solvent at high temperature, (2) crystallization of the polymer on a solid support by decreasing the temperature, (3) dissolution and elution of polymer fractions with different crystallizabilities by increasing the temperature. A schematic presentation of the TREF process is given in Fig. 2.1.

Typical solvents to be used in TREF are high boiling point solvents such as xylene, 1,2,4-trichlorobenzene (TCB), o-dichlorobenzene (ODCB), chloronaphthalene and others. Typical dissolution temperatures are between 120 °C and 160 °C and solution concentrations are around 0.5 wt%. Once the polymer is dissolved, the solution is loaded onto the TREF column which is filled with an inert support, e.g. sea sand, glass beads or stainless steel shots.

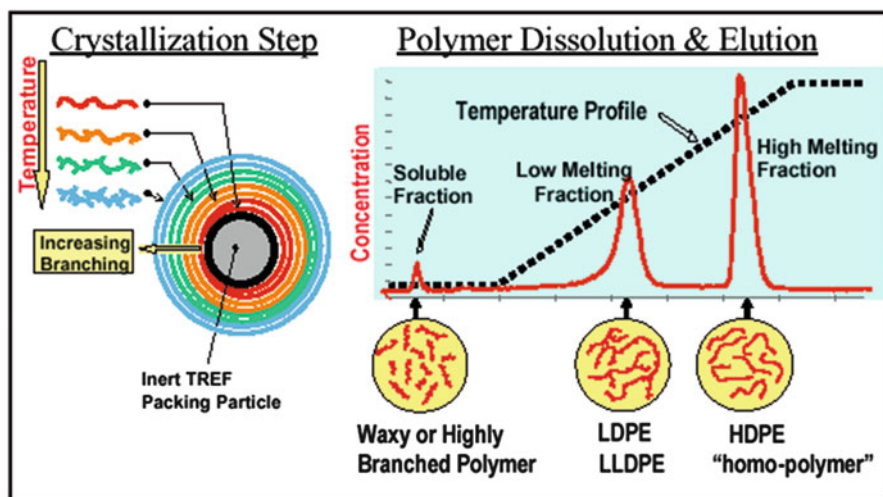


Fig. 2.1 Schematic presentation of the TREF process including the crystallization and the dissolution/elution steps

Alternatively, the polymer solution can be mixed with the support in a beaker or flask. In the next step, the temperature of the column (beaker, flask) is slowly decreased from high to ambient in order to crystallize polymer fractions out of the solution. At the highest temperature, the highly crystalline fractions will precipitate on the solid support followed by fractions of lower crystallinity. Accordingly, onion-type layers of polymer will be formed that have decreasing crystallinities from core to surface, as shown in Fig. 2.1. Non-crystallizing polymer fractions will remain in the solution. The type of crystalline layers will be influenced by the crystallization rate; in order to produce uniform layers crystallization rates as low as $0.1\text{ }^{\circ}\text{C}/\text{min}$ are used [10–14].

As has been pointed out earlier, crystallizability is (mainly) a function of chemical composition and molecular topology (branching). Accordingly, linear low density polyethylene (LLDPE) which exhibits a chemical composition distribution crystallizes with regard to the copolymer composition. Low density polyethylene (LDPE) which is a homopolymer but exhibits a branching distribution crystallizes with regard to the number and length of the branches [15].

After the crystallization step is completed, the TREF column contains a slurry of the solid support decorated with polymer sample layers. If crystallization was conducted in a beaker/flask, the slurry is now filled into the TREF column. The next step is the dissolution/elution step. A constant flow of solvent (mobile phase) produced by a standard HPLC pump is applied to the column and all soluble material is eluted. Typical flow rates are $0.5\text{--}2\text{ mL}/\text{min}$. At ambient temperature, the 'soluble fraction' consisting of (amorphous) material that did not crystallize elutes; see Fig. 2.1. By slowly increasing the temperature of the column and the mobile phase ($0.5\text{--}5\text{ }^{\circ}\text{C}/\text{min}$), the crystallized outer layers start to dissolve and elute

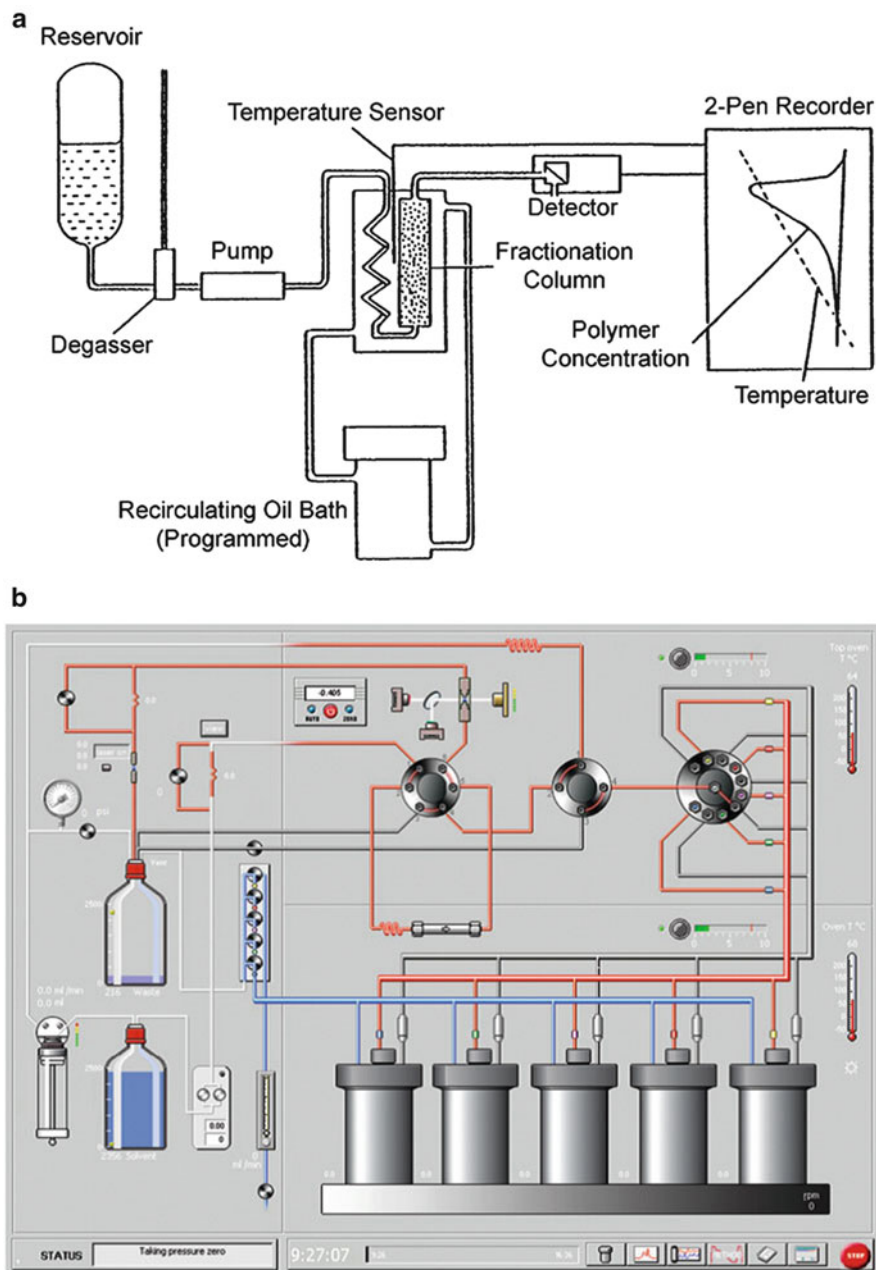


Fig. 2.2 Schematic diagram of analytical TREF (a) and fully automated Polymer Char instrument (b) (reprinted from [16] and [9] with permission of Springer Science + Business Media)

from the column. Accordingly, elution takes place with increasing temperature in the direction of increasing crystallizability. The latest eluting fractions have the highest crystallizability (lowest comonomer content, lowest degree of branching). The elution process is monitored by standard concentration detectors such as infrared (IR) and evaporative light scattering detectors (ELSD); however, more detailed information can be obtained when additional molar mass sensitive detectors, such as a viscometer (Visco) or light scattering (LS) detector, are used [10–14].

Over the years, different (mainly home-built) instruments have been used; for example see the schematic diagram in Fig. 2.2a [16] or instrument in [17]. Today, the most common instrument is the fully automated TREF instrument produced by Polymer Char, Valencia, Spain; see the schematic diagram in Fig. 2.2b.

Typical TREF curves for olefin block copolymers showing the influence of the α -olefin content in the hard block on the crystallizability are presented in Fig. 2.3. Kuhlman and Klosin investigated the block composition of PE multiblock copolymers as a function of different catalyst systems [18]. The block composition was tuned by a combination of hard and soft catalysts and diethylzinc (DEZ) as chain shuttling agent. With different catalyst compositions, the α -olefin content increased and the crystallization curves moved to lower temperatures from run A to run G. The amorphous part of the samples could not be resolved and eluted at the lowest temperature as a narrow peak.

As can be seen in Fig. 2.3, the TREF experiment produces a plot of elution temperature vs. concentration (wt%) of eluting fraction. For linear copolymers such as LLDPE, the elution temperature is directly proportional to copolymer composition. This has been shown by Boisson and co-workers for LLDPEs containing different comonomers [19]. As is shown in Fig. 2.4, for ethylene copolymers with propene, 1-hexene, 1-octene and 1-octadecene as comonomers, linear calibration curves were obtained. At the same molar composition the TREF dissolution temperature decreased with increasing branch length. Octene and hexene copolymers produced identical calibration curves.

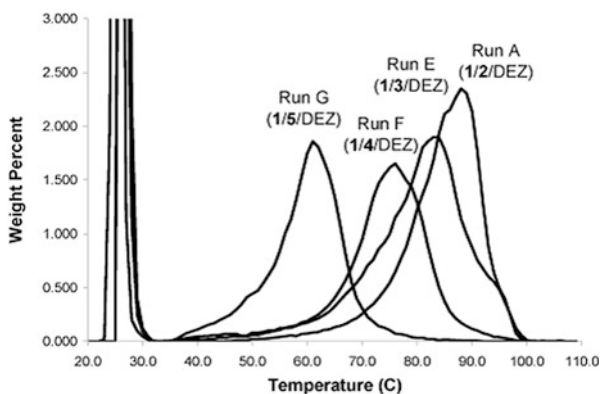


Fig. 2.3 The influence of α -olefin content in the hard block on polymer solubility as shown by TREF separation; sample code indicates catalyst composition (reprinted from [18] with permission of the American Chemical Society)

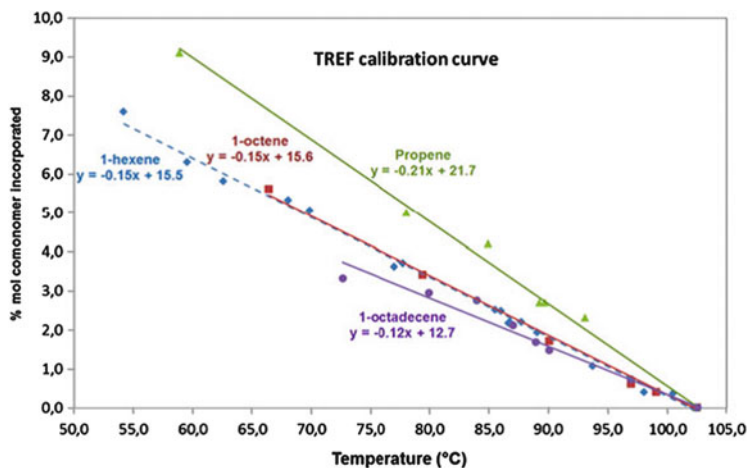
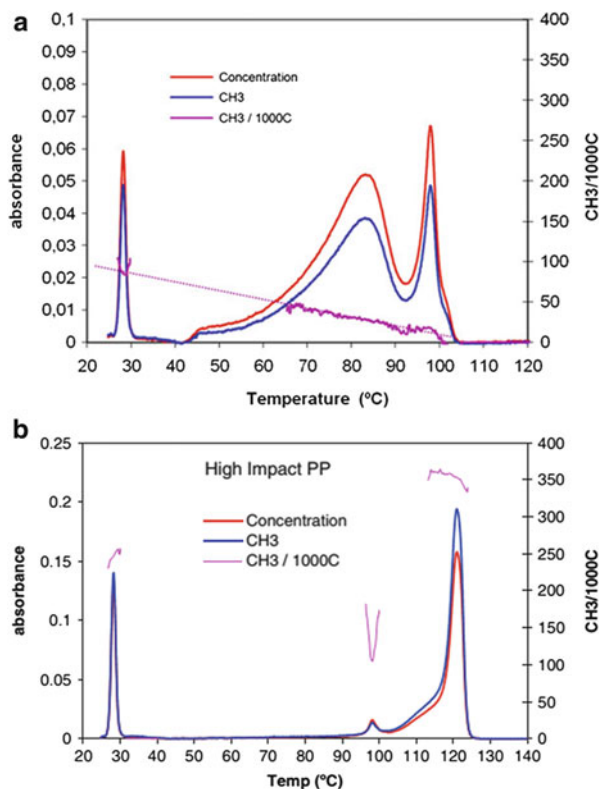


Fig. 2.4 TREF calibration curves for different ethylene copolymers (reprinted from [19] with permission of Wiley-VCH)

The elution in TREF has been shown to be independent of molar mass above 10 kg/mol [1, 2]. As an alternative to the calibration of TREF with well characterized polymer standards, a composition sensitive detector can be used, as has been demonstrated by Monrabal [20, 21]. Using a state-of-the-art IR detector with two simultaneous signals, one signal is used for total concentration while the other signal measures the methyl absorption, which is indicative for comonomer content. The ratio of the two signals gives the $\text{CH}_3/1,000\text{C}$ value for a typical LLDPE; see Fig. 2.5a. Assuming that the sample has no long chain branches, the value corresponds directly to the copolymer composition. It is remarkable that the $\text{CH}_3/1,000\text{C}$ calibration curve shows a linear dependence on elution temperature. The composition detector is particularly important in cases where the crystallization behaviour is influenced by copolymer composition and other parameters such as tacticity and branching. A good example for such a situation is the fractionation of high impact polypropylene copolymers (IPCs) where the IR detector reading provides copolymer composition irrespective of polypropylene (PP) tacticity; see Fig. 2.5b [9]. Other detector options are the online viscometer and the multiangle laser light scattering (MALLS) detectors that provide direct molar mass information.

As has been pointed out earlier, TREF is one of the workhorses of the polyolefin industry for characterization of polyolefins with respect to crystallizability. A typical procedure is to fractionate a complex polyolefin by TREF, isolate the fractions and subject them to a range of analyses including size exclusion chromatography (SEC) for molar mass and FTIR/NMR for chemical composition. Other approaches include the analysis of the crystalline structure by X-ray diffraction (XRD) and the thermal properties by differential scanning calorimetry (DSC).

Fig. 2.5 TREF analysis of a LLDPE with an IR detector for composition (a) and TREF analysis of an IPC using the same detector (b) (reprinted from [9] with permission of Springer Science + Business Media)



A few representative applications of TREF are reviewed as follows. The slow crystallization of PE in extended mode occurs only below molar masses of 2,000 g/mol, as shown by the analysis of TREF fractions using Raman spectroscopy in longitudinal acoustic mode (LAM) and DSC by Tomba et al. [22]. Chain folding takes place at higher molar masses. For a narrow molar mass range, independent crystallization was observed, in contrast to broad molar mass ranges where co-crystallization occurs in the case of polyolefin blends. These results indicated that crystallizable sequences really existed, and could be attributed to chain folding and co-crystallization phenomena. A perfect tool for the direct examination of the distribution of crystallizable sequences length was the Raman technique in LAM mode. DSC was limited only to samples where narrow distributions of crystallizable sequences were expected.

Hassan et al. [23, 24] correlated the preparation procedure of the Ziegler–Natta catalyst, the co-catalyst type, catalyst pretreatment and polymerization conditions with the tacticity of resulting PP by using SEC, NMR and TREF. Zhang and co-workers [25] studied the fractionation of random copolymers of propylene and ethylene by P-TREF, and carried out subsequent analysis of P-TREF fractions by SEC, ^{13}C NMR, DSC and wide-angle X-ray diffraction (WAXD) analysis. Copolymer molecules with varying compositions and molar masses were found in TREF

fractions. Random copolymers of propylene and 1-butene were synthesized by Zhang with Ziegler–Natta catalysts and the molecular microstructure and crystallization behaviour were correlated [26]. Relatively uniform microstructures with long isotactic polypropylene (iPP) sequences and isolated 1-butene comonomer units were found by analysis of TREF fractions using CRYSTAF, SEC and ^{13}C NMR. The increase in 1-butene content decreased the melting temperatures of the copolymers; therefore, higher temperature fractions contained less 1-butene content. Two LLDPE samples (comonomers 1-butene and 1-hexene) with similar densities were fractionated by van Reenen and co-workers. The melt flow index (MFI) values and comonomer contents were measured and the TREF fractions were analysed by high resolution solution and solid state NMR [27]. The type of crystallinity differed significantly in spite of similar degrees of crystallinity for both polymers. Insight into the detailed microstructure as provided by the hyphenation of TREF with NMR was not accessible otherwise. The same group reported on the fractionation of propylene–ethylene random copolymers by P-TREF. The fractions were subsequently analysed by CRYSTAF, DSC, ^{13}C NMR, HT-SEC and WAXD [28]. Their conclusion was that the incorporation of comonomers inhibited crystallization and the increase in ethylene content decreased the crystallization and melting points of the copolymers.

Suzuki et al. investigated the effect of the tacticity distribution on the thermo-oxidative degradation behaviour of PP by using TREF, NMR and thermographic analysis (TGA) [29]. It has been shown that atactic PP is more stable due to the hindered abstraction reaction of tertiary hydrogen. The abstraction of tertiary hydrogen was the rate-determining step in PP degradation and its dependence on tacticity distribution was correlated to the rate of degradation of PP. Therefore, the presence of more meso sequences in the chain will enhance the rate of thermo-oxidative degradation. Gupta et al. developed structure–property relationships for LLDPE by varying the length of short chains and keeping similar overall branching contents [30]. Despite similar TREF profiles, the mechanical properties of the LLDPE films varied significantly which was attributed to the type of the comonomer. Shan and Hazlitt developed a ‘block index methodology’ by analysing P-TREF fractions by A-TREF [31]. The comonomer content of olefin block copolymer fractions was higher than that of fractions of random copolymers eluting at the same temperature. The block index methodology of Shan and Hazlitt revealed the degree of intrachain comonomer distribution of olefin copolymers.

A comparison of HT-HPLC, CRYSTAF and TREF results for the chemical composition distribution (CCD) of ethylene–acrylate (EA) copolymers was presented by Pasch and co-workers [32]. A combinatory investigation of NMR, TREF, DSC and scanning electron microscopy (SEM) techniques was employed by Wang and co-workers for studying the compositional heterogeneity, phase structure and melting behaviour of PP prepared by two spherical $\text{TiCl}_4/\text{MgCl}_2$ catalysts [33]. PP homopolymers, PE homopolymers and ethylene-co-propylene copolymers with different ethylene segment lengths were the main components of the reactor alloys prepared by complex ethylene–propylene (EP) copolymerization. A sample prepared by a different procedure was slightly different; it contained PP

homopolymer, EP segmented polymer and EP random copolymer. The mechanical properties of the different materials were correlated with the molecular architectures and phase structures of the products. Amer and van Reenen reported on the TREF fractionation of iPP to obtain fractions with different molar masses but similar tacticities [34]. The DSC results of the fractions indicated that the configuration (tacticity) and the molar mass of the PP strongly affected the crystallization behaviour.

Cross-fractionation techniques such as SEC-TREF or TREF-SEC were used for the deconvolution of bivariate MMD/CCD distributions of polyolefin copolymers. The results were used to identify the number of active catalyst sites and the relation of the type of active sites with the microstructure of polyolefins produced with multiple-site catalysts [35]. Model ethylene-1-butene and ethylene-1-octene copolymers were used to validate the approach. The correlation of molecular structure and mechanical properties of ethylene-1-hexene copolymer film grade resins produced by a metallocene catalyst by varying the molar mass and branching distribution was studied by Alamo and co-workers [36]. Molar mass fractionation was achieved by solvent/non-solvent techniques, while fractionation with respect to 1-hexene content was obtained by P-TREF. The hyphenation of TREF with SEC-FTIR offered a simple alternative to conventional and time-consuming methods for characterizing the compositional heterogeneity of IPCs [37].

The idea to combine different polyolefin fractionation methods to address the multiple molecular distributions was developed by Nakano and Goto; they combined TREF and SEC to address the bivariate distribution in chemical composition and molar mass [38]. The resulting instrument was the first fully automated instrument that combined the chemical composition fractionation by TREF and the subsequent molar mass analysis of the TREF fractions by SEC.

When combining SEC and TREF there are, in principle, two options: SEC-TREF or TREF-SEC. The SEC-TREF approach was followed by Aust et al. [39] to analyse a medium density PE, while Faldi and Soares used TREF-SEC for the fractionation of a LLDPE [40]. Shan et al. developed a custom-built TREF-SEC instrument [41] which was used later by Gillespie et al. for SEC-TREF experiments [42]. Yau demonstrated the potential of a 3D-SEC-TREF apparatus which was used for the investigation of polyolefin microstructures [43]. A refractive index (RI) detector, a LS detector and a dual wavelength IR detector were used as online detectors, as shown in Fig. 2.6.

Monrabal and co-workers [44] pioneered the development of a user-friendly automated cross-fractionation apparatus (TREF-SEC) to fully characterize polyolefins with bivariate distributions; see Fig. 2.7. Short chain branching distributions have been analysed as a function of molar mass. The instrument was based on the design of a TREF 300 unit. The concentration detector employed is a dual band IR4 infrared detector. Further online detectors, such as methyl-sensitive IR sensors, Visco and LS detectors, can be added to enhance the amount of information.

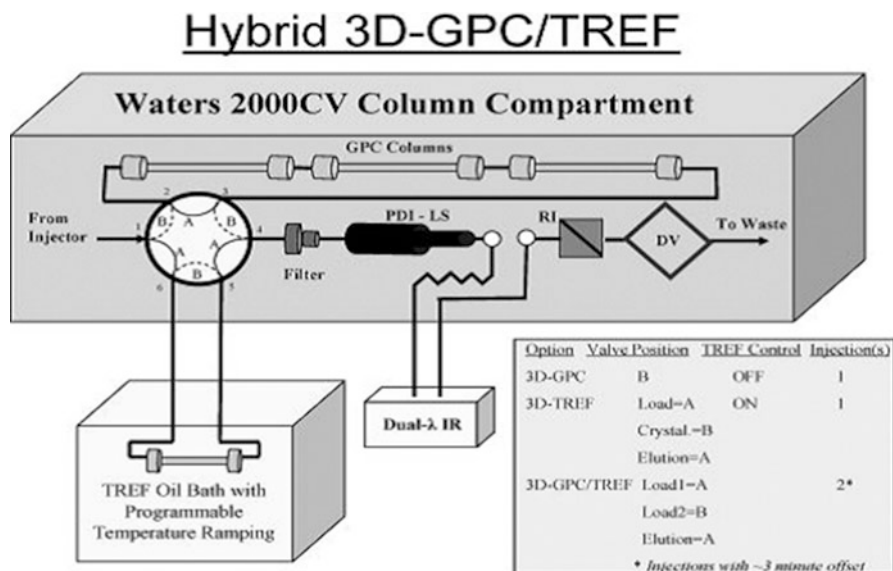


Fig. 2.6 Configuration of a hybrid 3D-SEC-TREF system (reprinted from [43] with permission of Wiley-VCH)

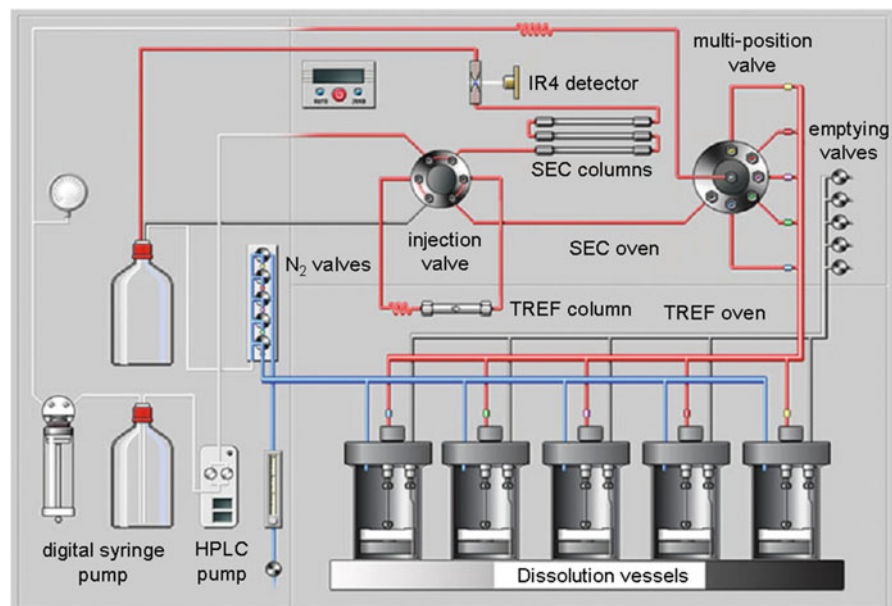
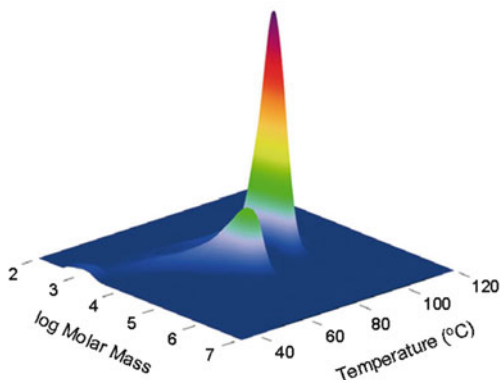


Fig. 2.7 Schematic diagram of an automated cross-fractionation instrument. Injection valve shown in 'load' position A; 'inject' position marked as B (reprinted from [44] with permission of Wiley-VCH)

Fig. 2.8 MMD \times CCD surface plot of a two-component PE blend (reprinted from [45] with permission of Polymer Char, Valencia, Spain)



In the TREF fractionation part, there are five stainless steel vessels equipped with internal filters and magnetic stir bars for dissolution and the subsequent sequential analysis. Dissolution of the sample is achieved by heating the TREF oven to 150 °C. The injection valve is moved to the ‘load’ position in order to load typically 1–3 mg of the sample into the TREF column through an internal filter. The injection valve is kept at the load position in the next step when crystallization of the sample is carried out. After complete crystallization and segregation of the polymer in the TREF column, a discontinuous elution at increasing temperature steps is carried out. A predefined dissolution time at each temperature is given for different fractions. The injection valve is then switched to the ‘inject’ position to elute the dissolved polymer fractions from the TREF column into the SEC column set. The flow through the TREF column is stopped again after elution of the given fraction by switching the injection valve to the ‘load’ position. The oven temperature is increased for dissolution of the next fraction. This process allows molar mass analysis of the TREF fractions that are collected with respect to increasing crystallinity. The final chromatogram is recorded by an IR4 infrared detector and the oven temperature signals are plotted against the raw IR signals. As a result of the cross-fractionation process, a 3D plot can be obtained, where the TREF elution temperature is plotted against the molar mass (from SEC) and the IR detector intensity (as a measure of concentration); see Fig. 2.8.

2.1.1 Fractionation of Ethylene–Octene Copolymers [46]

Ethylene–octene (EO) copolymers are one of the most important commercial polyolefin materials. EO copolymers constitute a significant share of the total market of LLDPE. With a total polyolefin market of more than 120 million tons, LLDPE has a market share of more than 17 %, with an increasing tendency to replace LDPE [47].

The higher tensile strength, superior impact and puncture resistance of LLDPE makes it more popular than LDPE. Thinner films of LLDPE can be produced

without compromising on strength, thus saving material and reducing costs. The toughness of LLDPE opens new horizons of application areas. The major share in global applications of LLDPE is film applications that include food and non-food packaging, shrink/stretch film and non-packaging applications. Metallocene or single-site catalysts revolutionized LLDPE research. New resins were synthesized that allow faster and more stable operations along with improved downgauging of films. Processing of LLDPE grades is also facilitated by improved and more effective methods. Today, major application areas of LLDPE are agricultural greenhouse films, multi-layer cast stretch films, lamination packaging films and medium to heavy duty bags.

2.1.1.1 Aim

An important step in the development of new or improved materials is the correlation of molecular structure and material properties. For molecular structure elucidation of complex polyolefins, TREF has been shown to be an invaluable tool. For LLDPE, TREF fractionation produces copolymer fractions that differ in comonomer content. These fractions are then analysed by spectroscopic methods (chemical composition, microstructure), SEC (molar mass) and calorimetric methods (melting and crystallization behaviour) for the development of structure–property correlations. A very useful approach is the online combination of TREF and FTIR spectroscopy, which will be discussed in the present application.

2.1.1.2 Materials

- *Polymers.* Ethylene-1-octene copolymers: sample 1 is a commercial random copolymer, sample 2 is a laboratory product. PE homopolymer (SRM1484a from the National Institute of Standards and Technology, Gaithersburg, USA; M_w 119.6 kg/mol). Eicosane

2.1.1.3 Equipment

- *TREF system.* CRYSTAF-TREF 200+ (Polymer Char, Valencia, Spain).
- *Detector.* FTIR flow cell (Polymer Laboratories, Church Stretton, UK), 1 mm optical path length, 70 μ L volume, CaF_2 windows. The cell was placed in a TENSOR 27 FTIR spectrometer (Bruker, Rheinstetten, Germany).
- *Solvent.* TCB stabilized with 2,6-di-*tert*-butyl-4-methylphenol (BHT).
- *TREF column temperature.* Temperature gradient between 140 °C and 25 °C.
- *TREF sample concentration.* 40–150 mg in 20 mL TCB per reactor vessel.

2.1.1.4 Preparatory Investigations

One of the challenges that TREF presents is to extract quantitative compositional information on the copolymers from the TREF elution profile. The raw data are presented as a plot of TREF elution temperature vs. eluate concentration. The correlation between the TREF elution temperature and the copolymer composition (wt% comonomer) can be obtained in different ways. Typically, a set of well defined copolymers with narrow CCDs and known compositions (from NMR) is measured by TREF and the peak maximum elution temperature for each sample is determined. This peak maximum elution temperature is then plotted against the wt

% comonomer to give a suitable calibration curve. Quite frequently, copolymer composition is expressed as the number of methyl groups per 1,000 carbons ($\text{CH}_3/1,000\text{C}$).

A much more feasible approach is the ‘real time’ measurement of the copolymer composition using an online FTIR detector. In this case, the analysis relies on the measurement of the absorption bands of the backbone methylene groups (at $2,855\text{ cm}^{-1}$ and $2,926\text{ cm}^{-1}$) corresponding to the total concentration and the methyl groups (at $2,874\text{ cm}^{-1}$ and $2,957\text{ cm}^{-1}$) corresponding to the concentration of the comonomer [48, 49]. As the intensities of the IR absorption bands do not directly correspond to concentration, a calibration of the FTIR data must be conducted. In the present case, blends of a linear PE and a low molar mass hydrocarbon (e.g. eicosane) as well as well defined single-site catalyst resins were used. It is known that for high molar mass linear PE the methyl chain ends contribute little to the visible complexity of the spectrum. Thus, the linear PE provided the total polymer concentration (CH_2) while the endgroups of the hydrocarbon provided the methyl group concentration (CH_3). Figure 2.9 shows expanded IR spectra of the linear PE and the hydrocarbon with corresponding peak deconvolutions to determine the polymer concentration and the methyl content.

Based on the analysis of the corresponding absorption bands, the polymer concentration ($[\text{C}]$) and the methyl content ($[\text{CH}_3]$) can be monitored as a function of the elution temperature. From these concentrations, the branch frequency (BF) can be calculated using Eq. (2.2).

$$\text{BF} = (14,000 \times [\text{CH}_3]) / (15 [\text{C}] - 14n [\text{CH}_3]) \quad (2.2)$$

n : depends on monomer, for octene $n = 5$

The BF is a direct measure for the LLDPE copolymer composition.

2.1.1.5 Measurement and Evaluation

It is known that both cooling and heating rates influence the TREF results. These parameters must, therefore, be selected very carefully. For the present LLDPE

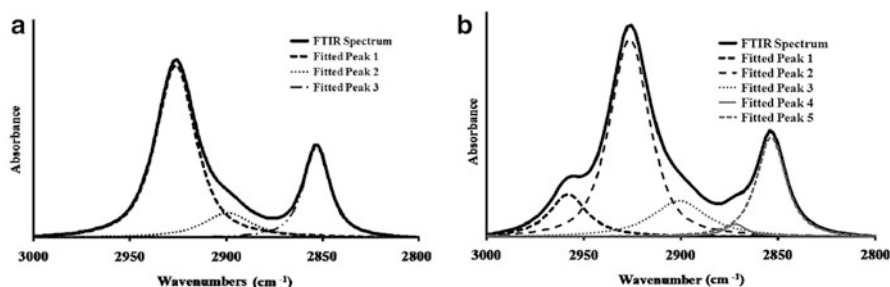


Fig. 2.9 Expanded IR spectra of linear PE (a) and eicosane (b) with peak deconvolutions for the methylene and methyl absorption bands, the shoulder at $2,900\text{ cm}^{-1}$ is a CH_2 combination absorption (reprinted from [46] with permission of Wiley-VCH)

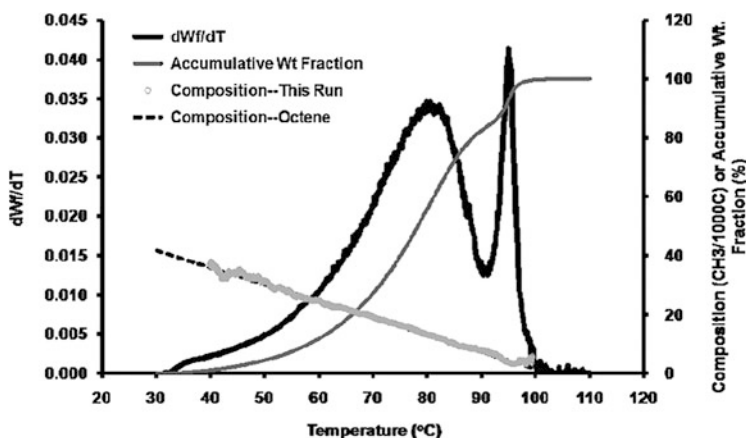


Fig. 2.10 TREF-FTIR profile of a random EO copolymer (reprinted from [46] with permission of Wiley-VCH)

samples, a cooling rate of $0.20\text{ }^{\circ}\text{C}/\text{min}$ was used; the heating rate was $0.25\text{ }^{\circ}\text{C}/\text{min}$. For the elution step, a flow rate of $0.75\text{ mL}/\text{min}$ was used.

The TREF-FTIR curve of a random EO copolymer is presented in Fig. 2.10. ‘dWf/dT’ is the differential mass per temperature increment; the accumulative weight fraction is calculated based on the mass profile. The comonomer content is expressed as $\text{CH}_3/1,000\text{C}$.

Figure 2.10 shows a typical TREF profile with a component that elutes at high temperature, producing a sharp elution peak and a range of components that elute in a broad peak between $30\text{ }^{\circ}\text{C}$ and $90\text{ }^{\circ}\text{C}$. A different TREF profile is obtained for a blocky EO copolymer produced by chain shuttling technology, see Fig. 2.11 [50]. This sample shows no elution peak at high temperature but a broad elution peak between $30\text{ }^{\circ}\text{C}$ and $90\text{ }^{\circ}\text{C}$. Different from the random sample, the olefin block copolymer exhibits a narrow elution peak at $25\text{ }^{\circ}\text{C}$.

The TREF curve of the random EO copolymer is quite representative for a LLDPE. The online FTIR detection shows that the octene content of the copolymer decreases with increasing TREF elution temperature. The highest eluting fraction does not contain octene and is, therefore, PE. The elution temperature of $96\text{ }^{\circ}\text{C}$ is in agreement with linear (high density) PE. The copolymer components eluting between $30\text{ }^{\circ}\text{C}$ and $90\text{ }^{\circ}\text{C}$ are due to EO copolymer molecules with different EO contents. The lowest eluting fractions have an octene content of about $40\text{ CH}_3/1,000\text{C}$. It is interesting to note that the TREF elution temperature is linearly dependent on the octene content of the copolymer. This makes it very easy to produce a calibration curve that stretches towards higher octene contents. The online FTIR detection also provides the total concentration of the sample components. Figure 2.10 indicates that the present sample contains about 10 % of PE.

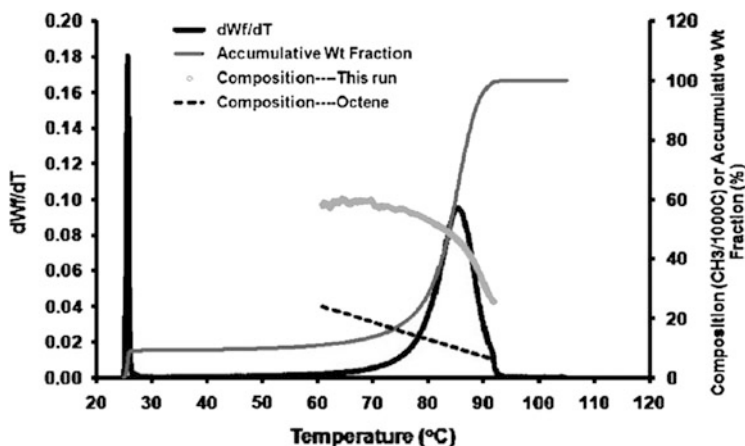


Fig. 2.11 TREF-FTIR profile of a blocky EO copolymer (reprinted from [46] with permission of Wiley-VCH)

A different type of TREF behaviour is seen for the blocky EO copolymer in Fig. 2.11. There is no component (PE) eluting beyond 90 °C. As in the previous case, the copolymer fractions elute in agreement with their octene content. A narrow TREF elution peak at 25 °C indicates that the sample contains material that did not crystallize in the crystallization step. The elution step starts at 25 °C and the ‘soluble fraction’ elutes first from the TREF column. This soluble material contains copolymer molecules with high octene contents and may even contain (amorphous) polyoctene (this comprises about 10 % of the total sample). It is an important limitation of TREF that only the crystallizable material can be fractionated. The fractionation of all components irrespective of the crystallizability can be achieved by means of column-based interaction chromatography as will be shown in Part 3.

Another remarkable feature of Fig. 2.11 is the difference between the actually measured octene content and the calibration curve that was obtained from the random EO copolymer sample. The figure clearly shows that the real octene content at a given elution temperature of the block copolymer is significantly higher than it is for the random copolymer. This is clear proof of the fact that the crystallization/elution temperature is not only influenced by the ‘bulk’ octene content but also by the microstructure (blockiness, type of branches) [31].

2.1.2 Fractionation of Impact Polypropylene Copolymers [37]

Another unique class of complex polyolefins is heterophase ethylene–propylene copolymers (EPCs). The major advantage of this class is improved low temperature impact strength of PP, therefore, they are frequently referred to as ‘Impact PP copolymers (IPCs)’. The common procedure for IPC production is via a two-reactor

sequential gas-phase polymerization in the presence of a Ziegler–Natta catalyst [51]. A complex mixture of reaction products is formed that ranges from amorphous random EPCs to crystalline iPP. This wide range of reaction products is attributed to the sequential polymerization procedure and the heterogeneous nature of the catalyst. Different monomer sequence distributions and sequence lengths lead to varying degrees of crystallinity. Accordingly, EPCs are semi-crystalline to varying extents [52–54] and are also referred to as EP block copolymers [55–57], although this terminology is misleading, regarding the nature of the mixture of end products obtained.

The distribution of ethylene and propylene sequences, the sequence lengths and the tacticities determine the final properties of IPC. Therefore, the detailed characterization of IPCs is an important subject, focusing on fractionation as well as spectroscopic analysis. Structural parameters of bulk EPCs have been investigated using ^{13}C -NMR as a method of choice [58]. The information on comonomer contents, distribution of monomers and tacticity could also be obtained by FTIR [59]. DSC is the method of choice to study the melting and crystallization behaviour of IPC. DSC is able to distinguish random copolymers from blends and block structures found in EPCs [60]. The complexity of IPC products makes fractionation techniques an integral part of the characterization protocol. Separation of the different components have been achieved by analytical and preparative TREF [52, 55, 57, 61, 62]. The hyphenation of TREF fractionation with ^{13}C -NMR, DSC and FTIR allows a comprehensive characterization of impact PP but it is a time-consuming procedure.

2.1.2.1 Aim

The present application describes the preparative TREF fractionation of a commercial IPC that is followed by a detailed investigation of the molecular structure of the fractions. In addition to NMR, DSC and SEC as the standard analytical methods, coupled SEC-FTIR shall be used to analyse the chemical composition as a function of molar mass.

2.1.2.2 Materials

- *Polymers.* Non-stabilized commercial IPC from SASOL Polymers (Secunda, South Africa) with the following bulk properties: ethylene content 10.5 mol%, isotacticity 88.8 % (mmmm), M_w 354 kg/mol, molar mass dispersity 3.18.

2.1.2.3 Equipment

- *TREF system.* In-house built preparative TREF apparatus. For crystallization, 3 g of polymer, ca. 2 wt% Irganox 1010 (Ciba Speciality Chemicals, Switzerland) and 300 mL of solvent were placed in a glass reactor and dissolved at 130 °C. The reactor was transferred to an oil bath maintained at 130 °C. As the crystallization support, pre-heated sea sand (white quartz; Aldrich, South Africa) was added to the reactor. The reactor was cooled at a rate of 1 °C/h. A stainless steel column was packed with the crystallized mixture and transferred to a modified GC oven. The temperature of the oven was increased at a steady rate

while pre-heated solvent was pumped through the column. Fractions were collected at pre-determined intervals, solvent was evaporated, fractions were recovered by precipitation in acetone and then finally dried to a constant weight.

- *Solvent.* Xylene
- *TREF column temperature.* Temperature gradient between 130 °C and 30 °C.
- *TREF sample concentration.* 3 g of polymer in 300 mL of solvent.
- *SEC.* PL 220 high temperature chromatograph (Polymer Laboratories, Varian Inc., Church Stretton, UK) at 150 °C equipped with three 300 × 7.5 mm i.d. PLgel Olexis columns and a differential RI detector. BHT stabilized TCB was the eluent at a flow rate of 1 mL/min. Sample concentration was 0.5 mg/mL in TCB and injection volume in all cases was 200 µL. Narrowly distributed polystyrene (PS) standards (Polymer Standards Service GmbH, Mainz, Germany) were used for calibration.
- *FTIR spectroscopy.* Attenuated total reflectance (ATR) measurements were recorded on a Nicolet Nexus 670 FTIR spectrometer (Thermo Electron, Waltham, USA) with a SensIR ATR attachment, equipped with a diamond reflective crystal, incidence angle of 45°. Spectra recorded from 4,000 to 650 cm⁻¹ were obtained from a collection of 64 scans at a resolution of 2 cm⁻¹.
- *DSC.* Mettler 822 DSC instrument (Mettler Toledo, Greifensee, Switzerland), calibrated with indium metal according to standard procedures, heating rate of 10 °C/min from 25 °C to 200 °C. Second heating cycle data were used for thermal analysis calculations. Measurements were carried out in a nitrogen atmosphere.
- *NMR.* 600 MHz Varian^{unity} INOVA NMR spectrometer (Varian Inc., Palo Alto, USA) operating at 125 MHz for carbon at 120 °C, 5 mm PFG switchable broadband probe, samples were prepared to a concentration of 6 wt% in deuterated tetrachloroethane (Aldrich, South Africa), 90° flip angle of approximately 6 µs, continuous proton decoupling, acquisition time 1.8 s, pulse delay time 15 s.
- *SEC-FTIR.* PL XT-220 (Polymer Laboratories, Church Stretton, UK) operating at 140 °C was coupled to a solvent evaporation FTIR interface LC-Transform (Series 300, Lab Connections, Carrboro, USA), stage and nozzle temperatures 160 °C and 150 °C, respectively, transfer line temperature 150 °C, solutes deposited on heated germanium disc and subsequently analysed by FTIR, analysis of SEC-FTIR results using Omnic software package (Thermo Electron, Waltham, USA).

2.1.2.4 TREF Fractionation

The preparative TREF fractions of the sample were collected at 30 °C, 60 °C, 80 °C, 90 °C, 100 °C, 110 °C, 120 °C and 130 °C. Figure 2.12 depicts the weight distribution ($W_i\%$) and weight fraction per temperature increment ($W_i\%/\Delta T$) of the eight P-TREF fractions. The 30 °C fraction and fractions eluting in the range 110–130 °C constitute the largest weight percentage of sample 3V, as is shown by the fractionation diagram. The principle of TREF fractionation is based on crystallizability; therefore, fractions collected at 30 °C are expected to be

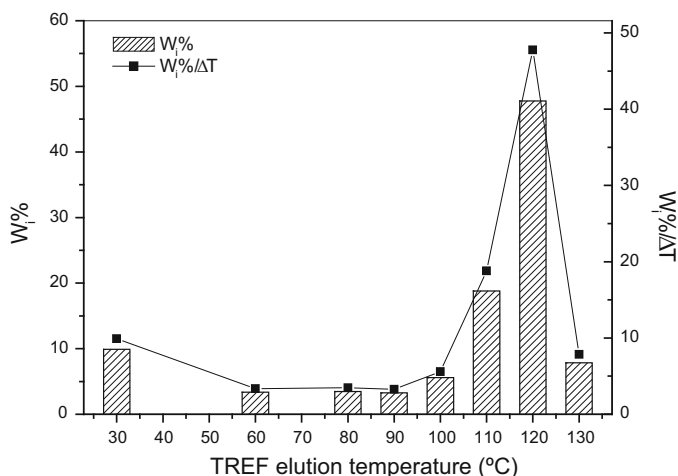


Fig. 2.12 Weight distribution and weight fraction per temperature increment for the TREF fractions of IPC (reprinted from [37] with permission of Wiley-VCH)

amorphous, while highly crystalline fractions are expected at higher temperatures (around 120 °C). The fractions obtained between these two extreme temperatures are assumed to be semi-crystalline with compositional differences. All fractions were analysed by DSC, ^{13}C -NMR and SEC-FTIR for determination of their chemical composition and thermal properties.

The relationships established by Ray et al. [63] and Randall [64] were used to calculate the comonomer contents and monomer sequence distributions from NMR; see Table 2.1. The method described by Kanezaki et al. [65] was used to obtain the isotacticity (% mmmm) data for the PP part; see Table 2.2.

The results indicate that the TREF fractionation was governed by decreasing comonomer content and increasing isotacticity. The fractionation also depended upon the increasing sequence length; the average length (n_x) of both ethylene and propylene sequences increased with increasing elution temperature. The first four fractions have high concentrations of PE and EP diads which indicate the linking of ethylene and propylene segments to some extent. On the other hand, the concentration of PE and EP diads becomes virtually zero in the highest eluting fractions. Therefore, higher eluting fractions consist of long iPP homopolymer sequences along with a small amount of PE homopolymer.

The fraction obtained at 30 °C contains equal amounts of ethylene and propylene with a high number of EP junctions, indicating the strong presence of EP random copolymers. However, some atactic PP and ethylene homopolymer may also be present. The higher temperature fractions that elute at 60 °C, 80 °C and 90 °C contain long sequences of both ethylene and propylene along with a fair number of EP junctions. This indicates that longer segments of propylene and ethylene are linked. The sequential gas-phase polymerization cannot produce true block structures; hence these are called ‘blocky’ copolymers.

Table 2.1 ¹³C-NMR monomer sequence analysis and tacticity data of the bulk 3V sample and its TREF fractions (reprinted from [37] with permission of Wiley-VCH)

Sample	P	E	PP	PE/EP	EE	PPP	PPE/EPP	EPE	EEE	EEP/PEE	PEP	%mmmm
3V	89.52	10.48	86.36	6.34	7.32	84.19	3.63	1.70	5.75	3.18	1.58	88.82
30 °C	49.55	50.45	34.43	30.23	34.39	49.39	0.14	0.02	25.78	13.42	1.80	24.70
60 °C	45.11	54.89	34.15	21.92	43.87	28.74	11.64	4.73	37.56	12.43	1.65	36.13
80 °C	44.46	55.54	38.29	12.32	48.99	37.74	3.96	3.11	44.47	7.47	1.00	64.91
90 °C	54.31	45.69	52.66	3.31	43.83	54.26	0.04	0.01	42.25	2.37	0.06	71.21
100 °C	90.27	9.73	89.96	0.63	9.11	89.37	0.90	0.00	8.50	0.02	0.11	85.74
110 °C	94.85	5.15	94.85	0.00	4.37	91.86	2.99	0.00	2.81	0.00	0.00	86.54
120 °C	99.39	0.61	99.39	0.00	0.61	99.39	0.00	0.00	0.61	0.00	0.00	91.52

Table 2.2 The Average ethylene (n_E) and propylene (n_P) sequence lengths of sample 3 V and its TREF fractions (reprinted from [37] with permission of Wiley-VCH)

Sample	n_E	n_P
3V	3.31	28.86
30 °C	5.41	3.32
60 °C	5.00	4.12
80 °C	8.95	7.21
90 °C	27.51	32.84
100 °C	29.99	287.23
110 °C	n.d.	n.d.
120 °C	n.d.	n.d.

n.d. not determined

2.1.2.5 Fraction Analysis and Evaluation

The molar masses of the bulk polymer and the TREF fractions were analysed by SEC. As can be seen in Fig. 2.13, a number of fractions exhibit monomodal MMDs while others are bimodal. Such molar mass bimodality might indicate compositional heterogeneity. This has frequently been observed for the mid-elution temperature fractions of IPC fractionated by TREF [62, 66, 67] where semi-crystalline EPC and PP homopolymer co-elute due to the isotacticity distribution found in PP [62, 68]. PP homopolymer will not elute entirely at high TREF temperatures, because PP fractions of lower isotacticity will become soluble within the same lower temperature range of the semi-crystalline EPC phase of corresponding crystallizability.

Additional evidence for the complexity of the TREF fractions is obtained from the thermal behaviour, as shown in Fig. 2.14 for the DSC heating curves.

As expected, no melting or crystallization is observed for the 30 °C fraction. This fraction is amorphous and contains random EP rubber and (perhaps) some low molar mass PP with a low isotacticity. The higher temperature fractions (110 °C and 120 °C) have a single, distinct melting peak around 160 °C, which confirms the monomodality of fractions containing predominantly iPP. The fractions eluting at lower temperatures (60–100 °C) show bimodalities with two melt endotherms, indicating the presence of two distinct crystallizable components. Furthermore, the fractions show an increase in melting temperatures for both endotherms from the 60 °C fraction to the 100 °C fraction, which is a clear indication of an increase in crystallinity of both components with increasing elution temperature. The appearance of two melt endotherms for the mid-elution fractions confirms the assumption derived from the SEC curves that these fractions exhibit a significant compositional heterogeneity. SEC, however, separates according to molecular size and not chemical composition. Therefore, bimodality in the SEC profiles does not conclusively prove a chemical heterogeneity. One way to overcome this problem is to couple SEC with a selective detector such as FTIR, as has been shown in Sect. 2.1.1. In the present case, however, the LC-Transform interface is used instead of a flow cell. The operation of this device has been described elsewhere and a number of important applications have been presented [14, 69]. The advantage of this

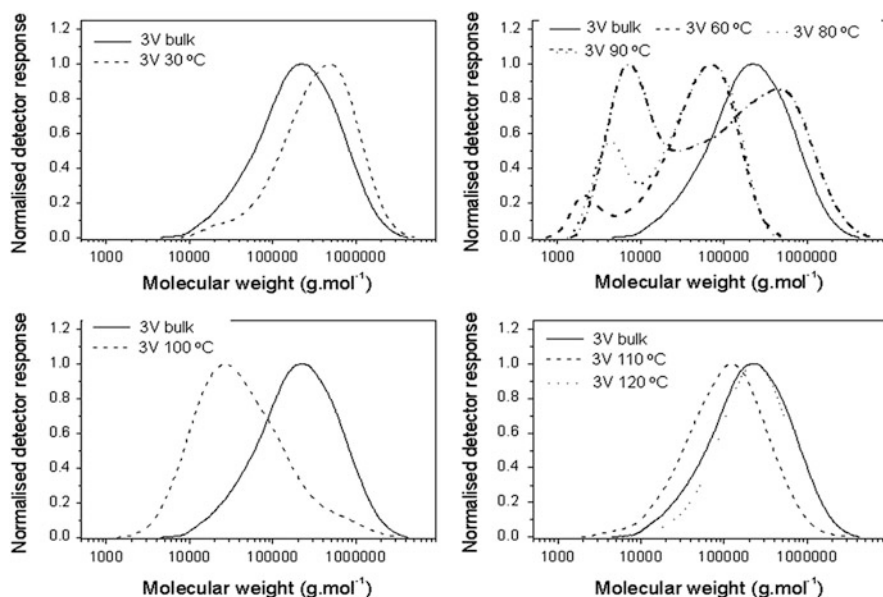


Fig. 2.13 Molar mass distributions of the bulk IPC and the TREF fractions (reprinted from [37] with permission of Wiley-VCH)

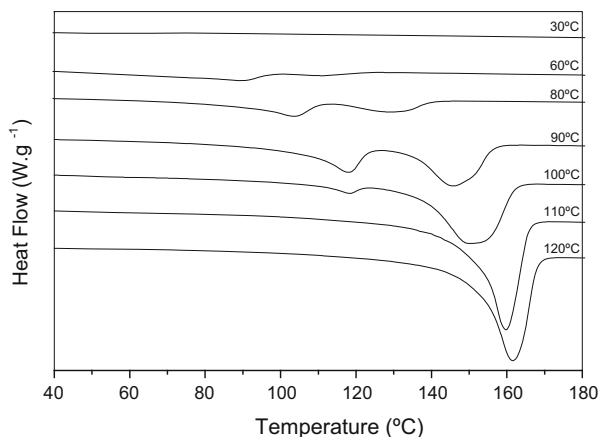


Fig. 2.14 Melt endotherms of the TREF fractions of IPC as obtained by DSC (reprinted from [37] with permission of Wiley-VCH)

approach is that not only can two wavelengths (e.g. for total concentration and methyl group content) be monitored, but for each SEC slice a complete FTIR spectrum is generated. The results of the SEC-FTIR analysis of the TREF fractions are summarized in Figs. 2.15 and 2.16.

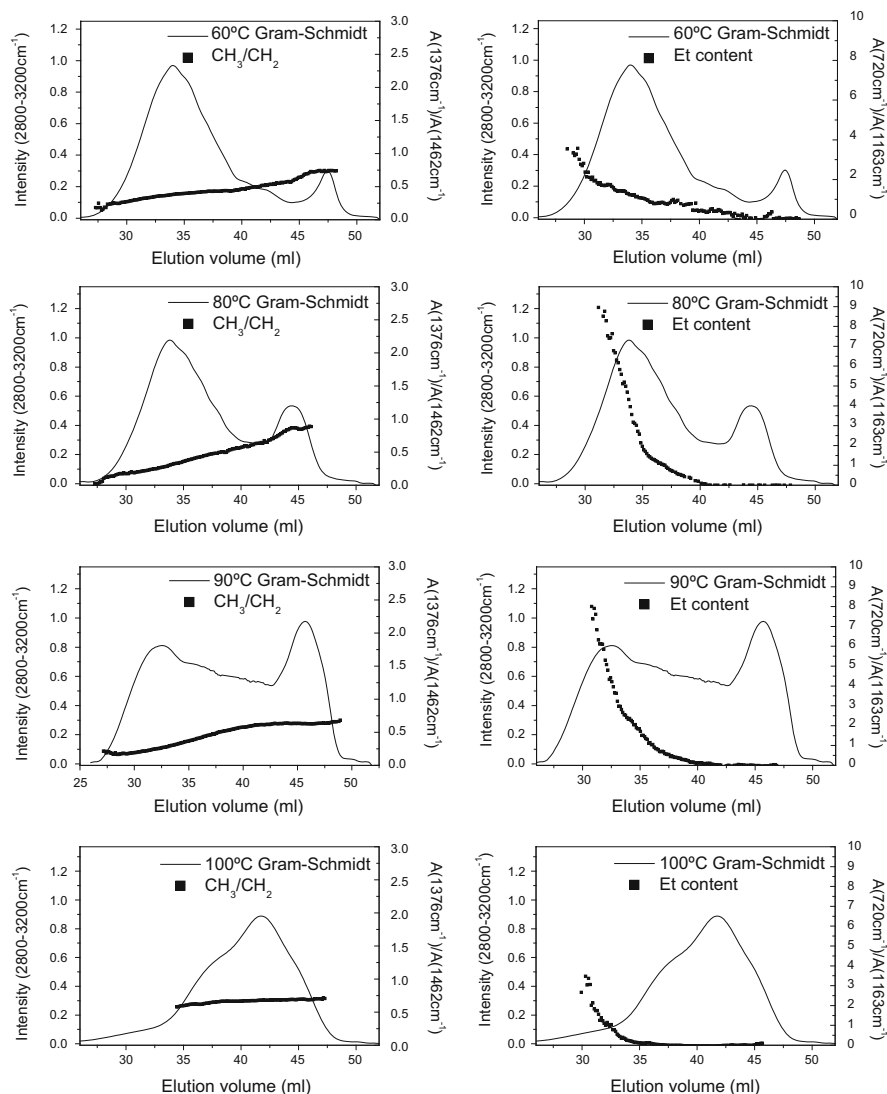


Fig. 2.15 SEC-FTIR analysis of the ethylene and propylene distribution within the 60 °C, 80 °C, 90 °C and 100 °C TREF fractions of IPC (reprinted from [37] with permission of Wiley-VCH)

The Gram-Schmidt plots represent the total FTIR absorption over the 2,800–3,200 cm^{-1} range of the spectrum. The shape of the plot resembles SEC curves, which show distributions of molar masses from higher to lower as the elution volume increases. In the Gram-Schmidt plot, CH_3/CH_2 corresponds to the distribution of propylene and 'Et content' corresponds to the ethylene content profile. The areas of the absorption bands at 1,376 cm^{-1} and 1,462 cm^{-1} correspond to CH_3 and CH_2 , respectively, and are used for quantification of the propylene content

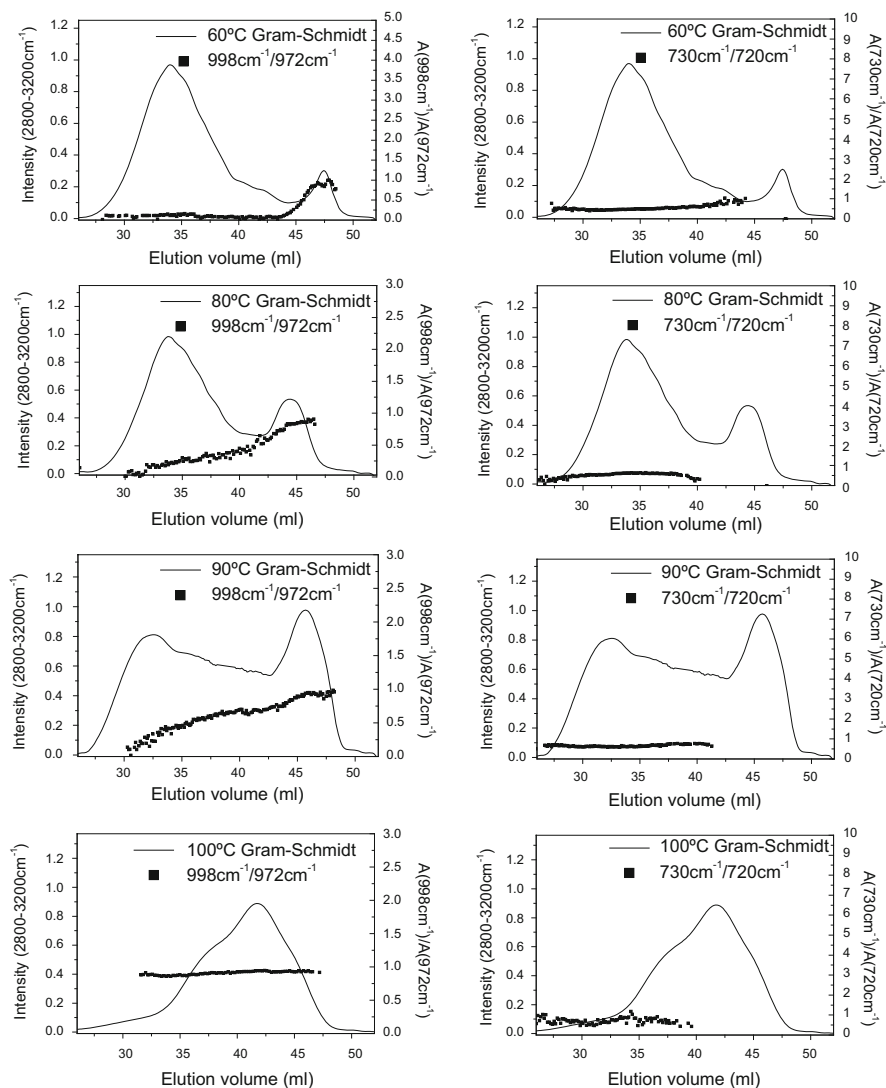


Fig. 2.16 SEC-FTIR analysis of the ethylene and propylene crystallinity distributions within the 60 °C, 80 °C, 90 °C and 100 °C TREF fractions of IPC (reprinted from [37] with permission of Wiley-VCH)

[70–72]. The total polymer concentration is measured by the intensity of the CH_2 band, whereas the presence of CH_3 groups indicates branching and is characteristic of PP units. The chain branching in PE may also result in the band at $1,378\text{ cm}^{-1}$; therefore, the validity of using the ratio of $1,378\text{ cm}^{-1}/1,462\text{ cm}^{-1}$ was investigated. This was achieved by constructing the ethylene profile across the molar mass curve. The ratio of the areas of the bands at 720 cm^{-1} and $1,163\text{ cm}^{-1}$

was used for the ethylene content quantification within an EP block copolymer [73]. The gradual increase in the CH_3/CH_2 ratio across the bimodal MMDs is observed for the first three fractions eluting at 60 °C, 80 °C and 90 °C, respectively. This indicates the higher propylene content in the lower molar mass component; see Fig. 2.15. The ethylene content decreases gradually from the higher molar mass side of the distribution until it reaches zero within the lower molar mass region, as indicated by the ratios of the $720\text{ cm}^{-1}/1,162\text{ cm}^{-1}$ bands. This is a clear indication that ethylene is only present in the higher molar mass components and the band at $1,378\text{ cm}^{-1}$ represents the methyl groups in PP only.

There is a visible difference in the compositions of the lower and high molar mass components of the bimodal distribution. PP homopolymers are the sole component of the lower molar mass region, in contrast to the high molar mass part which is composed of EPCs with varying monomer distributions. The ethylene-rich copolymers appear on the higher molar mass side. The propylene content increases towards the lower molar mass side of the distribution. The 100 °C fraction forms the transition between blocky copolymers and iPP fractions eluting at higher temperature, as predicted by ^{13}C -NMR. The Gram–Schmidt curve constructed from the CH_3/CH_2 ratio shows lower values for regions of higher molar mass (low elution volume) compared to the low molar mass region, indicating the differences in the propylene content in both regions of the MMD. This is a clear sign that the propylene content is lower in the region of higher molar masses. The results are in good agreement with the ratio of $720\text{ cm}^{-1}/1,163\text{ cm}^{-1}$, which decreases to zero in the direction of higher elution volumes. The presence of EPC in the higher molar mass shoulder in the 100 °C fraction is therefore confirmed by SEC-FTIR analysis. The two melt endotherms in each of these fractions determined by DSC analysis suggest the presence of both crystalline ethylene and propylene segments. The specific crystalline entities for both monomers are associated with specific IR bands; therefore, the construction of ethylene and propylene crystallinity profiles should be possible from SEC-FTIR. The 998 cm^{-1} and 841 cm^{-1} bands are associated with long repeating monomer units in the crystalline 3_1 helix of PP [74–77]. The short helix segments are associated with the 972 cm^{-1} band of the FTIR spectrum. There is a linear correlation between the intensities of the 998 cm^{-1} and 841 cm^{-1} bands and the density of PP as a measure of its crystallinity [78]. PP tacticity can, therefore, be determined by the ratio of the 998 cm^{-1} and 972 cm^{-1} absorption bands, providing the degree of spectral crystallinity in PP.

FTIR spectroscopy also provides information on the relative crystallinity of ethylene segments in EPCs along with propylene segments. The 720 cm^{-1} band originates from long methylene sequences. With the increase in crystallinity of PE, the intensity of the 730 cm^{-1} component increases at the cost of splitting of the 720 cm^{-1} band [79, 80]. The band at 730 cm^{-1} is recognized as a true crystallinity band [75]. Therefore, the relative crystallinity in PE is related to the ratio of the band intensities at 720 cm^{-1} and 730 cm^{-1} [80–82]. The ratios of $998\text{ cm}^{-1}/972\text{ cm}^{-1}$ and $730\text{ cm}^{-1}/720\text{ cm}^{-1}$ are constructed across the Gram–Schmidt

curves to examine the distribution of ethylene and propylene crystallinity across the molar mass profiles; see Fig. 2.16.

The low elution volume component of the 60 °C fraction shows a very low level of propylene isotacticity or crystallinity. The higher elution volume component (corresponding to lower molar mass) shows higher ratios of $998\text{ cm}^{-1}/972\text{ cm}^{-1}$, indicating the presence of PP homopolymer. Crystalline ethylene sequences are present only in the lower elution volume component, which can be identified as the semi-crystalline EPC component of this fraction. The absence of the 730 cm^{-1} and 720 cm^{-1} absorption bands resulted in the discontinuation of this profile within the higher elution volume component of the distribution.

In the case of the 80 °C and 90 °C fractions, the ratio of the $998\text{ cm}^{-1}/972\text{ cm}^{-1}$ absorption bands increases across the bimodal distribution towards higher elution volumes where PP homopolymer is located. Ethylene crystallinity is only seen in the lower elution volume component. This is the region where EPC elutes. Therefore, crystalline ethylene and propylene segments are found in the EPC phase and highly crystalline isotactic PP is found in the lower molar mass PP phase. The crystalline ethylene segments of the EPC are represented by lower temperature melt endotherms in the DSC heating curve. The higher temperature melt endotherm in the DSC heating curve is due to melting of propylene segments of EPC and PP homopolymer. A uniform propylene concentration is detected in the 100 °C fraction across the Gram–Schmidt curve. The higher elution volume end of the PP homopolymer component of preceding fractions and this fraction show similar values for the $998\text{ cm}^{-1}/972\text{ cm}^{-1}$ ratio. There is only a slight variation at the lower elution volume shoulder, where EPC elutes, as indicated by the CH_3/CH_2 ratio. Crystalline ethylene segments are also detected only in the low elution volume shoulder of the Gram–Schmidt plot. The SEC-FTIR results for ethylene and propylene crystallinity agree well with DSC results on the thermal behaviour of the fractions.

2.1.3 Analysis of Thermo-oxidatively Degraded Polypropylene [83]

Polyolefins are susceptible to degradation which takes place throughout the life cycle of the material. Degradation occurs during polymerization, processing, application and recycling. It influences the polymer properties, thereby limiting the lifetime of the materials and leading to economic losses [84, 85]. To reduce the degradation of a particular material, the sources of degradation and the degradation pathways must be understood. This is a strong motivation to search for new analytical methods to analyse and monitor the degradation of polyolefins [86]. A particular aspect is the increasing importance of polymer recycling with the aim not to downgrade the material.

One can distinguish between photo-oxidative and thermo-oxidative degradation. Polyolefins can also be attacked by strong acids [87]. The generally accepted free radical oxidation model of polyolefins involves radical initiation, propagation and termination reactions [88, 89]. Following an initiation reaction, which usually

results from the thermal or photo-initiated dissociation of chemical bonds, alkyl radicals react with molecular oxygen to form peroxy radicals [90]. The oxygen-containing functionalities like ketones, alcohols, carboxylic acids, esters and γ -lactones are due to the propagation reactions [91–96]. Fractionation is an important approach to obtain information about degradation and the distribution of degradation products. CRYSTAF and TREF separate semi-crystalline polyolefins based on crystallizability. These methods in combination with spectroscopic methods shall now be used for the analysis of degraded polyolefins.

2.1.3.1 Aim

In Sect. 2.1.2, the compositional heterogeneity of a commercial IPC was measured by hyphenation of TREF fractionation with SEC-FTIR analysis. The chemical composition as function of MMD of all fractions was determined. The morphological nature of the components was further confirmed by determination of ethylene and propylene crystallinity distributions across the MMDs.

In the present application, the thermo-oxidative degradation of IPC shall be addressed. IPC is degraded at different times and temperatures like in previous reports on PP and PP-1-pentene copolymers [97, 98]. The bulk sample analysis by SEC, FTIR, SEC-FTIR, CRYSTAF and DSC is used to monitor the process of degradation. A degraded sample is fractionated by P-TREF and the fractions are analysed for molar mass and chemical composition in order to obtain information on degradation of individual components of IPC. A comparison of two different IPC samples with regard to chemical composition will be presented. The degree of degradation as a function molar mass, chemical composition and crystallinity will be determined for the fractions of degraded materials. Finally, samples shall be evaluated and compared with respect to thermo-oxidative stability.

2.1.3.2 Materials

- *Polymers.* The bulk properties of two non-stabilized commercial IPCs from SASOL Polymers (Secunda, South Africa) are presented in Table 2.3 (samples were labelled 3V and 4V, O h indicates original samples before degradation). To prevent degradation during film extrusion and sample preparation, 0.05 % of phosphite processing stabilizer, Irgafos 168, was added for compounding of the materials. Dry-blending of the IPC powder and Irgafos 168 was followed by melt-blending at 200 °C on a Brabender PL 2000-6 single-screw extruder equipped with a 19 mm diameter screw, length-to-diameter ratio of 25 and screw speeds of 40–100 rpm. The extrudates were cooled and pelletized. Thin films (1 g of material, ca. 160 μ m) were prepared by compression moulding at 190 °C. A typical compression cycle consisted of melting of the pellets for 1.5 min and compression at 10–12 bar for another 1.5 min, with subsequent quench cooling in an ice/water mixture.
- *Accelerated oven ageing.* The thermo-oxidative degradation of thin films at 90 °C and 110 °C was accomplished in a heat-circulating oven with digital temperature control (SMC manufacturing, Cape Town, South Africa). The visual (for physical changes) and FTIR (for chemical changes) monitoring of the degradation followed the degradation process and samples were removed at

Table 2.3 Summary of the molecular properties of IPC samples 3V and 4V

Sample	[Ethylene] (mol%)	Isotacticity (%mmmm)	M_w (g/mol)	M_n (g/mol)	M_w/M_n	T_m (°C)	T_c (°C)	ΔH_m (J/g)
3V-0h	10.48	88.82	354,400	114,600	3.18	118.15	162.56	93.84
4V-0h	16.42	83.17	351,900	86,600	4.06	116.28	160.69	72.45

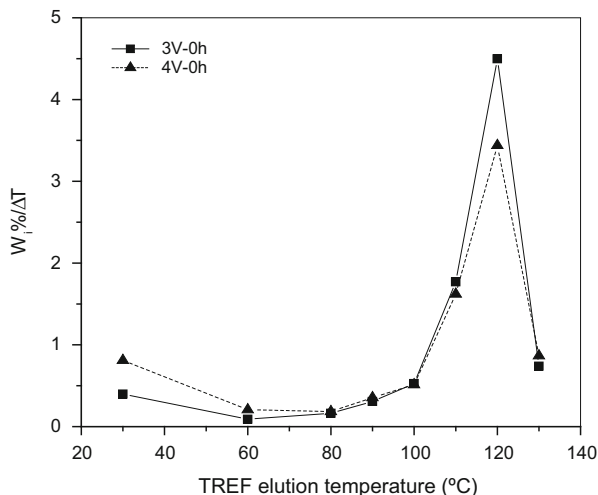
Ethylene content and isotacticity (%mmmm): determined by ¹³C-NMR; M_w , M_n and M_w/M_n measured by HT-SEC; T_m , T_m and ΔH_m measured by DSC

regular intervals for further analysis. The degradation process was discontinued when samples snapped or flaked on bending. The degraded films were homogenized by shredding the film into small pieces and re-melting into a single film for a very brief time. Films removed from the oven at advanced stages of degradation were brittle and shattered easily. Plasticity was, however, restored after the re-moulding process.

2.1.3.3 Equipment

- *SEC*. Polymer Laboratories PL 220 high temperature chromatograph (Polymer Laboratories, Church Stretton, UK) at 150 °C, equipped with three 300 × 7.5 mm i.d. PLgel Olexis columns and a differential RI detector. The eluent was TCB stabilized with BHT, at a flow rate 1 mL/min. Sample concentration was 0.5 mg/mL in TCB and the injection volume was 200 µL. Calibration was done with PS.
- *FTIR Spectroscopy*. Nicolet Nexus 670 FTIR spectrometer (Thermo Electron, Waltham, USA). Spectra were recorded from 4,000 to 650 cm⁻¹. Spectra were obtained from a collection of 64 scans at a resolution of 2 cm⁻¹.
- *DSC*. Mettler 822 DSC instrument (Mettler Toledo, Greifensee, Switzerland), calibrated with indium metal according to standard procedures, heating rate of 10 °C/min from 25 °C to 200 °C. Data obtained during the second heating cycle were used for thermal analysis calculations. Measurements were conducted in a nitrogen atmosphere.
- *NMR*. 600 MHz Varian^{unity} INOVA NMR spectrometer (Varian, Palo Alto, USA) operating at 125 MHz for carbon at 120 °C, 5 mm PFG switchable broadband probe, samples were prepared to a concentration of 6 wt% in deuterated tetrachloroethane (Aldrich, South Africa), 90° flip angle of approximately 6 µs, continuous proton decoupling, acquisition time 1.8 s, pulse delay time 15 s.
- *TREF*. In-house built preparative TREF apparatus. For crystallization, 3 g of polymer, ca. 2 wt% Irganox 1010 (Ciba Speciality Chemicals, Switzerland) and 300 mL of solvent were placed in a glass reactor and dissolved at 130 °C. The reactor was transferred to an oil bath maintained at 130 °C. As the crystallization support, pre-heated sea sand (white quartz; Aldrich, South Africa) was added to the reactor. The reactor was cooled at the rate of 1 °C/h. A stainless steel column was packed with the crystallized mixture and transferred to a modified GC oven. The temperature of the oven was increased at a steady rate while pre-heated solvent was pumped through the column. Fractions were collected at pre-determined intervals, solvent was evaporated, fractions were recovered by precipitation in acetone and then finally dried to a constant weight.
- *Solvent*. Xylene.
- *TREF column temperature*. Temperature gradient between 130 °C and 30 °C.
- *TREF sample concentration*. 3 g of polymer in 300 mL of solvent.
- *CRYSTAF*. CRYSTAF apparatus Model 200 (Polymer Char, Valencia, Spain). 20 mg of the sample was dissolved in 40 mL ODCB. Stainless steel reactors for crystallization were equipped with an automatic stirring and filtration device and crystallization was carried out under agitation. The dissolution at 160 °C was

Fig. 2.17 Crystallization curves of IPC samples 3V and 4V obtained by TREF ($W_i\%/\Delta T$) (reprinted from [83] with permission of Wiley-VCH)



followed by cooling to 100 °C for stabilization and then to 30 °C at a cooling rate of 0.1 °C/min. Fractions were collected automatically and an IR detector was used to determine the concentration of the solution at the chosen wavelength of 3.5 μm .

2.1.3.4 TREF Fractionation and Analysis of Non-degraded Samples

Samples were fractionated by preparative TREF and fractions were collected at 30 °C, 60 °C, 80 °C, 90 °C, 100 °C, 110 °C, 120 °C and 130 °C; see Fig. 2.17.

Although the maxima of the TREF curves at 120 °C are similar for the two samples, the intensity of the 4V crystallization peak is lower than that of sample 3V and a larger TREF soluble fraction at 30 °C is detected for sample 4V. The higher percentage of ethylene comonomer in sample 4V will result in larger amounts of non-crystallizable material.

To study the heterogeneity of the copolymers, TREF fractions were analysed by ^{13}C -NMR, SEC and DSC. The comonomer content and isotacticity data of the TREF fractions of the samples as obtained by ^{13}C -NMR are presented in Fig. 2.18a, b. In both samples, the isotacticity increases with increasing TREF elution temperature indicating that the fractionation of the PP phase is governed by tacticity. The ethylene content decreases in the same direction. Significant differences are found between the two samples. In parallel to the increasing isotacticity and decreasing comonomer content, the melting temperatures increase with increasing TREF elution temperature; see Fig. 2.18d. For the molar masses of the different fractions, as obtained by SEC, no clear trend can be observed. However, the soluble fraction appears to have the highest molar mass, see Fig. 2.18c.

Figure 2.18a shows that for both copolymers the ethylene content decreases towards higher elution temperatures. The first three fractions of copolymer 4V contain considerably higher concentrations of ethylene. The next four fractions of copolymer 4V are similar to copolymer 3V as far as ethylene content is concerned.

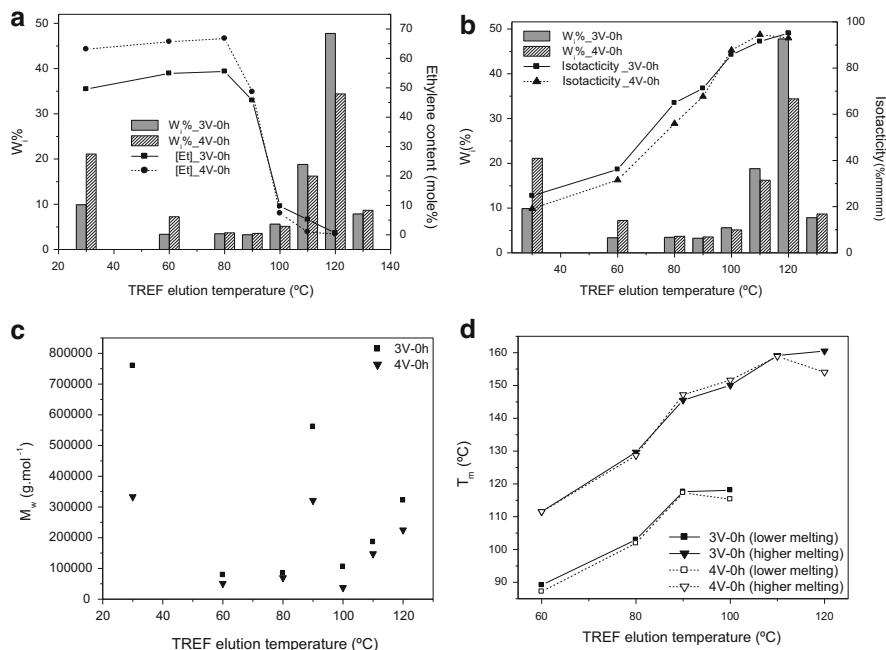


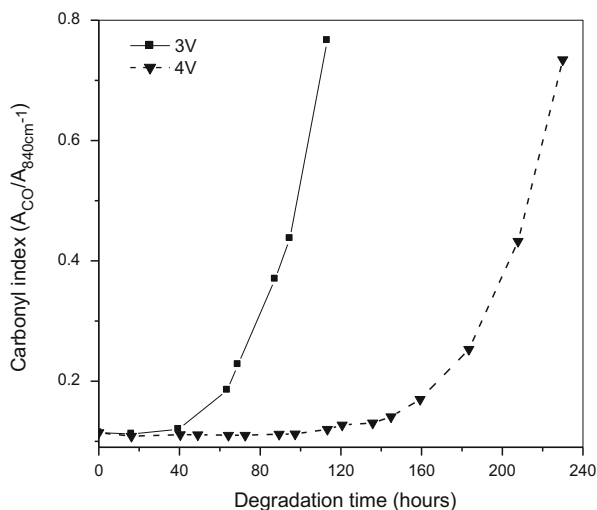
Fig. 2.18 Analytical results for the TREF fractions of IPC samples 3V and 4V, ethylene content (a), isotacticity (b), average molar masses M_w (c) and DSC melting temperatures (d) (reprinted from [83] with permission of Wiley-VCH)

It seems that random copolymer fractions incorporated the excessive ethylene comonomer introduced during polymerization. This introduces shorter segments of ethylene and propylene in the EP rubber (EPR) and ‘transition’ copolymers. Therefore, the nature of random and semi-crystalline EPCs should be more affected by higher comonomer contents compared to the PP matrix. This is in agreement with the polymerization process, where iPP is produced in the first reactor while the formation of EPCs takes place only in the second reactor. In DSC, two melt endotherms were observed in the 60–100 °C fractions of both samples, see Fig. 2.18d, indicating that the 60 °C, 80 °C, 90 °C and 100 °C fractions consist of co-eluting PP with lower isotacticity and semi-crystalline EP copolymers. The crystallizable ethylene sequences in the EPC phase correspond to the lower of the two melt endotherms, whereas the higher melt endotherm is due to the propylene sequences from both the EPC and PP homopolymer phases.

Table 2.4 summarizes the compositional differences between the two samples. The 30 °C fraction was identified as EPR. The co-eluting components of EPC and low isotacticity PP with short sequences of ethylene and propylene form the 60 °C and 80 °C fractions. The same constituents are present in the 90 °C and 100 °C fractions but with higher isotacticity of PP and longer ethylene and propylene

Table 2.4 Compositional heterogeneity of IPC samples 3V and 4V

Sample	T_c			
	30 °C	60–80 °C	90–100 °C	110–130 °C
	EPR + aPP	‘Transition’ EPC + low isotacticity PP	‘Blocky’ EPC + high isotacticity PP	Isotactic PP + PE
3V-0h	9.90	6.83	8.86	74.72
4V-0h	21.11	10.94	8.67	59.28

Fig. 2.19 Carbonyl index changes in IPC samples 3V and 4V (reprinted from [83] with permission of Wiley-VCH)

sequences. iPP is the major constituent of the 110–130 °C fractions, with traces of PE homopolymer.

2.1.3.5 Analysis of Degraded Bulk Samples

The accelerated thermo-oxidative degradation of thin films of samples 3V and 4V was executed under similar conditions. After predetermined times, samples of both grades were taken from the oven and analysed further. FTIR data and the progress of embrittlement of complete film areas were used for monitoring the progress of degradation. The differences in the embrittlement rate of both samples were compared. The 3V films showed faster embrittlement compared to sample 4V. The rate and extent of degradation of both samples was compared quantitatively by means of the carbonyl index. The carbonyl index was calculated as the peak height ratio of the maximum of the carbonyl band at 1,804–1,580 cm^{-1} and the reference band at 840 cm^{-1} ; see Fig. 2.19.

Copolymer 3V degraded at a faster rate and with a shorter induction time of about 40 h compared to sample 4V. Sample 4V showed signs of degradation in the form of gradual enhancement of the carbonyl index only after 100 h of ageing. A steady rate of degradation was observed for both samples after the induction period. However, the steeper slope of the carbonyl index curve of sample 3V indicates the

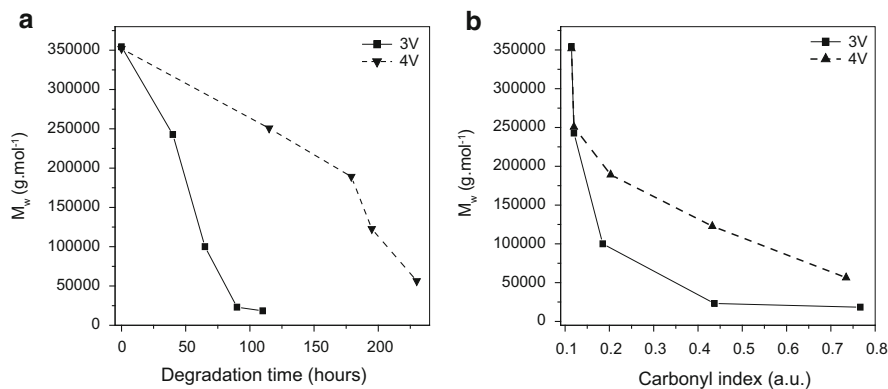


Fig. 2.20 Comparison of M_w decrease of samples 3V and 4V as a function of degradation time (a) and carbonyl index (b) (reprinted from [83] with permission of Wiley-VCH)

faster degradation rate compared to sample 4V. The decrease in M_w with increasing degradation time is presented in Fig. 2.20a. The M_w changes as a function of the carbonyl index (obtained with ongoing degradation) for both the samples are presented in Fig. 2.20b. The different rates of degradation can be seen clearly by changes in molar mass upon ongoing degradation, despite of the fact that the nondegraded samples have identical molar masses. The molar mass decrease to approximately 250,000 g/mol was noted during the first stages of degradation (up to 40 h and 115 h for samples 3V and 4V, respectively). However, the M_w decrease for sample 3V was considerably faster compared to sample 4V after longer degradation times. This confirms the higher degradation rates in the copolymer with lower contents of comonomer and isotacticity.

The thermal behaviour of the two samples is presented in Fig. 2.21, showing the changes in CRYSTAF T_c , as well as DSC T_c , T_m and ΔH_m .

The three molecular parameters, namely carbonyl index, molar mass and either CRYSTAF T_c or DSC T_c or T_m , can be combined to study the effect of molar mass and carbonyl concentration on the crystallization and melting temperature of the degraded copolymers; see Fig. 2.22a, b. The influence of degradation on the interrelationship between three seemingly independent parameters is clearly indicated by these presentations, irrespective of the different time scales of the degradation of IPC samples 3V and 4V.

2.1.3.6 TREF Fractionation and Analysis of the Degraded Samples

The degraded samples were recrystallized in TREF. The same fraction collection TREF profile as for the nondegraded samples was used. The nondegraded and degraded samples were compared at different degradation times with regard to the weight fractions per temperature increment ($W_i\%/\Delta T$); see Fig. 2.23. The crystallization peaks shifted to lower temperatures from 120 °C for nondegraded and

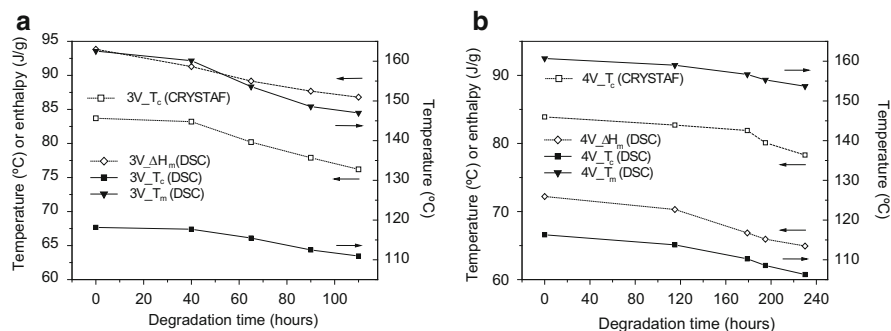


Fig. 2.21 Comparison of the changes in crystallization and melting behaviour as a function of degradation time for samples 3V (a) and 4V (b) (reprinted from [83] with permission of Wiley-VCH)

slightly degraded samples to 110 °C for samples degraded for longer times. CRYSTAF measurements show the selective degradation of the higher isotacticity fractions. The results are confirmed by the decrease in intensity and shift towards lower values for crystallization peak temperature along with an increase in the amount of material eluting at the lowest elution temperature.

The SEC results of selected fractions of the degraded samples are shown in Fig. 2.24. For the highest eluting fractions, the shifts in molar mass of the two samples are very similar. This is expected, because these fractions consist mainly of iPP. The 60–90 °C fractions exhibit bimodal distributions due to low isotacticity PP and EPC. As can be expected, little differences are observed between the samples in terms of molar mass changes of the low isotacticity PP component. The EPC component, however, shows slightly different molar mass shifts in the two samples. The most significant differences in the molar mass changes are, however, seen within the 30 °C fractions. These fractions consist mainly of EPR. The higher comonomer content and lower isotacticity of EPR of sample 4V seemingly make it more stable than sample 3V. The stability of the 60–90 °C fractions of sample 4V seems to be improved by the higher ethylene content.

The results indicate a longer induction period and slower increase in carbonyl functionalities, as well as a slower decrease in M_w for sample 4V. The delayed onset and slower oxidation rate in IPCs with higher ethylene content are attributed to the introduction of more stable ethylene units in the polymer chain. The number of tertiary PP carbons that can undergo dissociation reactions is believed to be eliminated by the presence of ethylene units. The presence of the 3_1 helix in crystalline PP promotes the bimolecular decomposition reaction that is of lower activation energy than the unimolecular decomposition occurring in more random conformations; hence, higher isotacticity of the PP unit also increases the rate of oxidation. The samples currently being studied have only small differences in ethylene content and isotacticity, and relatively large differences in the amount of amorphous material. Nonetheless, they show a considerable difference in their degradation behaviour. The analysis of the fractions of both copolymers by SEC

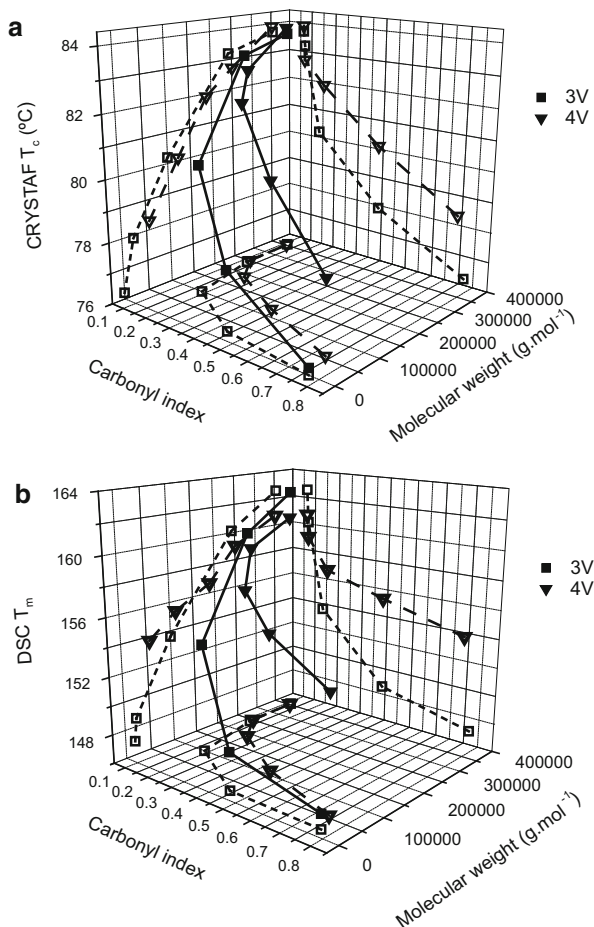


Fig. 2.22 Comparison of differences in the relationships between carbonyl index, molar mass and CRYSTAF T_c (a) and DSC T_m (b) for samples 3V (squares) and 4V (triangles) (reprinted from [83] with permission of Wiley-VCH)

and DSC agreed quite well. The 30 °C and 90 °C fractions of samples 3V and 4V show slight differences in their molar masses. The fractions collected at similar TREF elution temperatures for both products have almost identical T_m and T_c values. The similarity in distribution of isotacticity of the PP phase and the sequence length of ethylene and propylene of the EPC component of corresponding fractions of the two copolymers is illustrated by the results. However, weight percentages of the fractions eluting at corresponding elution temperatures are different for the two samples. For copolymer 4V, larger amounts of amorphous fractions (30–90 °C) and smaller amounts of more crystalline fractions (110 °C and 120 °C) are collected during P-TREF compared to product 3V. Similar amounts

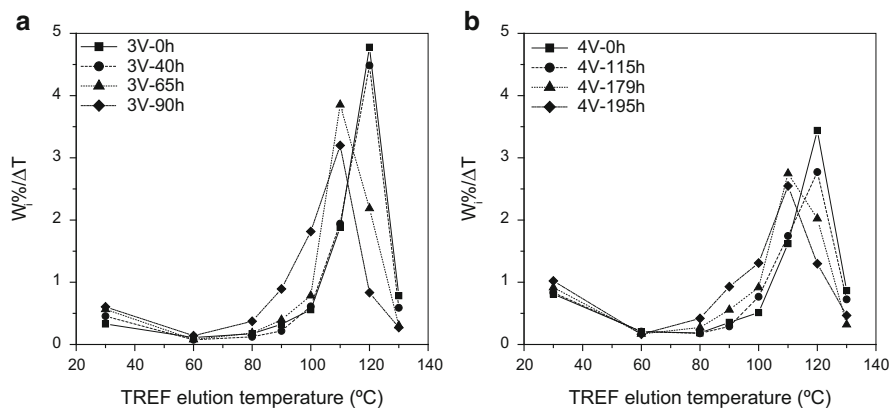


Fig. 2.23 TREF weight fraction per temperature increment curves ($W_i\%/\Delta T$) for the degraded samples 3V (a) and 4V (b) at different degradation times (reprinted from [83] with permission of Wiley-VCH)

were obtained for the middle fraction collected at 100 °C. The subsequent analysis of the fractions by ^{13}C -NMR, DSC, SEC and CRYSTAF demonstrated that the major constituents of the corresponding fractions of both products are the same; only the amounts differed.

Sample 4V showed a delayed induction and a slower oxidation rate. The reason for this behaviour is the higher ethylene content and lower isotacticity of the bulk sample. Further explanations of this behaviour include the relative amounts of the four major components within the two samples. Larger concentrations of amorphous EPR and transition EPC accompanied by a lower concentration of iPP were found in copolymer 4V by TREF analysis of the nondegraded sample. iPP degrades preferentially, for reasons explained earlier, despite of the presence of large amounts of amorphous material. Data from hyphenation of TREF fractionation with ^{13}C -NMR suggested that in the polymerization of sample 4V, the excess ethylene that is added during the second stage is located in the EPR and the transition EPC fractions.

The degradation behaviour of the two samples shows interesting trends. The most important factors that determine the degradation behaviour are the amount and distribution of ethylene in the four components of IPC. An increase in ethylene content induces higher chemical stability and a barrier effect of the comonomer in intrachain hydroperoxide formation. These effects account for the increase in oxidation induction time and stability. The morphology of IPCs is also affected by the amount of ethylene. The morphological variations include the shapes and sizes of the dispersed EPR phase and the nature of the segmented EPCs that act as compatibilizer at the interface between the EPR inclusions and the iPP matrix. The role of this interface is vital in the migration and combination of free radicals during the degradation of heterophase EPCs. It is therefore concluded that the stability differences between the two grades are attributed to their morphological disparity.

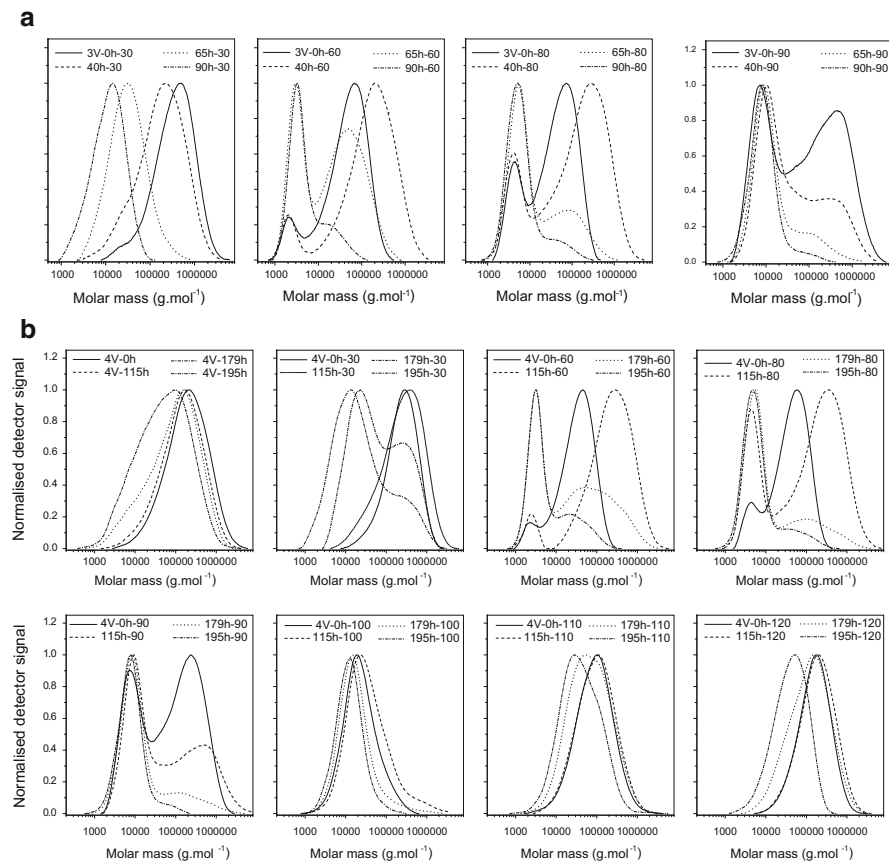


Fig. 2.24 Changes in molar mass distributions of TREF fractions from degraded samples 3V (a) and 4V (b). Sample codes are as follows: first number—degradation time in h, second number—TREF elution temperature (reprinted from [83] with permission of Wiley-VCH)

The unique morphology of these copolymers plays a very important role in governing the degradation, along with the effect of chemical composition. The study was extended to thicker specimens where oxygen diffusion is expected to play a greater role. FTIR microscopy and a conventional technique involving layer-by-layer milling followed by SEC, FTIR and CRYSTAF analyses were used to study the spatial heterogeneity within the copolymers 3V and 4V [99]. Details of hyphenation of TREF-SEC-FTIR are discussed in [100].

2.2 Crystallization Analysis Fractionation

Besides all the merits of TREF, one of the important shortcomings is the very long time that is required for the slow crystallization and elution steps. This makes a TREF experiment a very time-consuming procedure that requires from a few hours to a few days, depending on the experimental protocol. CRYSTAF was developed by Monrabal in 1999 to overcome this problem and to speed up the CCD analysis of olefin copolymers [8, 101]. CRYSTAF is based on the same principles of separation by crystallizability from dilute solutions but, instead of two steps—crystallization and elution, it makes use of only one step—crystallization. This crystallization takes place in a stirred vessel with no support. The polyolefin sample is dissolved at high temperature, followed by a slow decrease of the temperature of the solution. Depending on the composition of the sample, fractions of different crystallizability (chemical composition) precipitate out of solution at different temperatures.

The crystallization process is continuously monitored as a function of temperature using a suitable detector, typically a dual wavelength IR detector. Aliquots of the polymer solution are analysed by the detector after filtration through the internal filter in the vessel. The detector reading is assumed to provide relative concentration information. Consequently, a profile of polymer concentration in the solution as a function of temperature is obtained; it is termed as a cumulative CRYSTAF profile. As the temperature of the solution is decreased, an increasing fraction of polymer in solution crystallizes out and, accordingly, polymer concentration in solution decreases. Similar to TREF, a correlation between polymer concentration in solution at a given temperature and chemical composition is developed through a calibration curve. Copolymer standards with narrow CCDs are used to create the calibration curve for particular experimental conditions (cooling rate, comonomer type, solvent, etc.). The typical means of obtaining polyolefins with narrow CCDs are P-TREF fractionation or direct synthesis using single-site catalysts.

Polymer Char (Valencia, Spain) is the only supplier of CRYSTAF instrumentation; the schematic diagram of their commercial version is illustrated in Fig. 2.25. The instrument is equipped with five stainless steel crystallization vessels with stirrers and a temperature programmable oven for parallel analysis. A nitrogen line, a waste line and a sampling line with an inline filter are provided to all five vessels. A dual wavelength online IR detector is connected to the sampling line. The detector is also heated to 150 °C and polymer concentration in solution as a function of temperature is measured. A good solvent for the polymers such as TCB is used for dissolution of the sample, while keeping the concentration of the polymer in solution between 0.1 mg/mL and 1.0 mg/mL. Interchain interactions and co-crystallization could occur if higher concentrations are used. On the other hand, low concentrations can lead to poor signal-to-noise ratio (SNR). Experience and literature suggest that the most suitable stirring rate during dissolution and stabilization is 200 rpm. The stirring rate should be reduced to 100 rpm during crystallization. The Co-crystallization should be avoided by cooling at a very slow rate. A typical cooling rate is kept at 0.1–0.2 °C/min during the crystallization step.

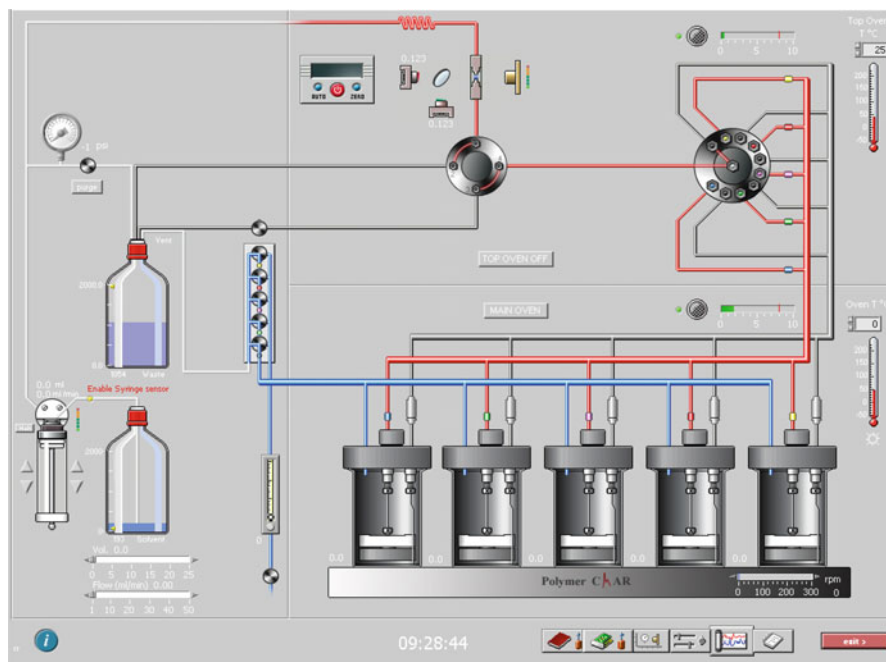


Fig. 2.25 Systematic diagram of a CRYSTAF instrument (Polymer Char, Spain) (screenshot from instrument)

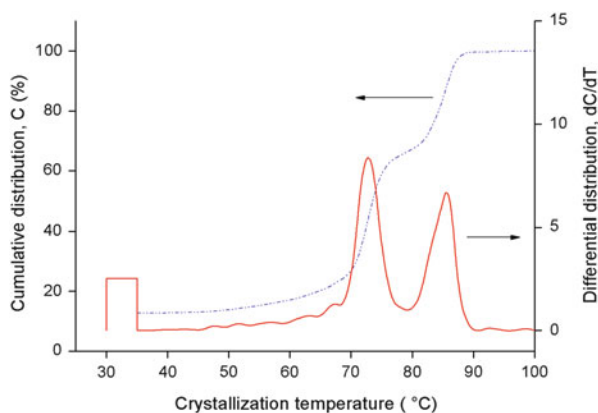


Fig. 2.26 Cumulative and differential CRYSTAF profiles of a blend of HDPE and PP

The differentiation of the integral CRYSTAF profile at each temperature provides the amount of polymer crystallizing at each temperature. The CRYSTAF plot presents the polymer crystallized as a function of temperature. It is the most widely used and lucid representation of CRYSTAF results. Figure 2.26 depicts the integral and differential profile for a blend of HDPE and PP. The molar mass of the polymer,

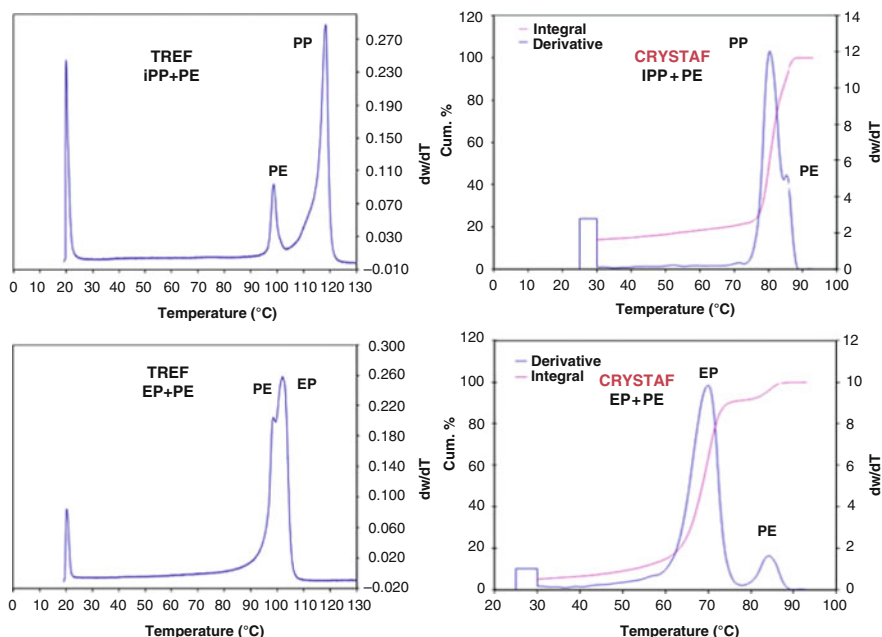


Fig. 2.27 TREF and CRYSTAF analysis of PE–PP combinations showing the different fractionation capabilities (reprinted from [9] with permission of Springer Science + Business Media)

the comonomer type and content, the cooling rate and co-crystallization effects must be taken into account for reliable CRYSTAF profiles, as is the case with TREF. Comprehensive reviews on crystallization-based techniques summarize the state of the art up to 2005 [12, 102]. More recent information is given in [9, 10].

As pointed out earlier, CRYSTAF was developed originally as a faster version of crystallization fractionation and it was assumed that TREF and CRYSTAF would produce similar results. This is not entirely correct, as can be seen from a comparison that was presented by Monrabal [9]. TREF data are generated in the dissolution step while CRYSTAF data refer to the crystallization step. Each step works differently, e.g. for iPP, PE and EP copolymers; see Fig. 2.27. In TREF, iPP and PE are adequately fractionated, with iPP eluting at a higher temperature. This is not the case in CRYSTAF due to the undercooling effect for iPP resulting in crystallization of iPP and PE at nearly the same temperature. On the other hand, CRYSTAF fractionates EP and PE adequately, while in TREF the resolution of this fractionation is rather poor.

2.2.1 Characterization of Homogeneous Ethylene–Octene Copolymers [103]

For the last 30 years LLDPE has been produced mainly using multiple-site (Ziegler–Natta, ZN) catalysts. These copolymers have broad (multimodal) CCDs, which has a strong impact on product performance. The CCD of olefin copolymers is also referred to as short chain branching distribution (SCBD).

The fractionation of EO copolymers by TREF has been discussed in Sect. 2.1.1. It has been shown that ZN LLDPEs contain a highly crystalline fraction of HDPE and fractions of very low crystallinity that have high comonomer contents.

2.2.1.1 Aim

In the present application, the CCD of homogeneous EO copolymers shall be analysed by CRYSTAF. Such LLDPEs are typically produced by using a single-site (constrained geometry) catalyst. The correlation between crystallization temperature and comonomer content shall be investigated and the data shall be used for calibrating CRYSTAF/TREF. Finally, the behaviour of these homogeneous LLDPEs shall be compared to a commercial ZN LLDPE.

2.2.1.2 Materials

- *Polymers.* A series of 17 samples of EO copolymers produced by Dow Chemical in a solution process with a constrained geometry catalyst, sample densities 0.868–0.935 g/cm³, melt indexes (at 190 °C, with 2.16 kg, according to ASTM D1238) are 0.5–30 dg/min.

2.2.1.3 Equipment

- *CRYSTAF system.* Commercial CRYSTAF instrument model 100 (Polymer Char, Valencia, Spain).
- *Detector.* Built-in dual wavelength IR detector with heated flow-through micro cell at 150 °C.
- *Solvent.* TCB.
- *Crystallization protocol.* Crystallization between 90 °C and 30 °C (in selected cases between 90 °C and 5 °C) at a rate of 0.2 °C/min.
- *Sample concentration.* 30 mg in 30 mL TCB.

2.2.1.4 Preparatory Investigations

As a first step of the investigation, the homogeneous EO copolymers were measured. Figure 2.28 shows the CRYSTAF curves of three representative samples. As expected, the samples exhibit monomodal and narrow crystallization profiles, which are a clear indication of their narrow CCDs.

The CRYSTAF results of all samples are summarized in Table 2.5 and compared to other analytical data.

The calculation of the weight and number average crystallization temperatures T_w and T_n , respectively, and the parameters measuring the broadness of the CCD, are as follows:

Fig. 2.28 CRYSTAF analysis of three homogeneous LLDPEs (reprinted from [103] with permission of J. Wiley & Sons)

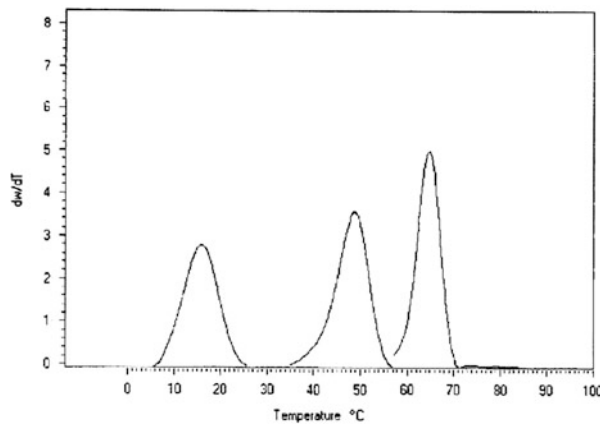
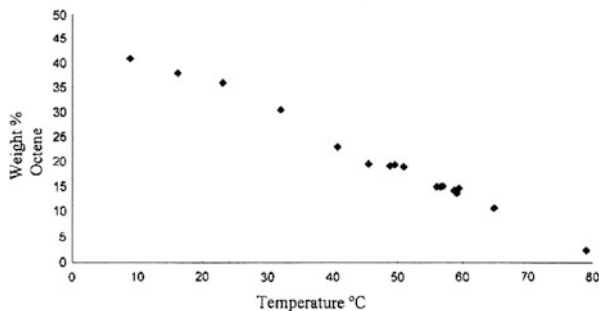


Table 2.5 CRYSTAF and analytical results for EO copolymer samples (reprinted from [103] with permission of J. Wiley & Sons)

T_c (°C)	T_w (°C)	Sigma	R	Weight % Octene	Density	M.I.
8.9	6.8	5.2	—	41	0.868	0.5
16.2	13.7	7.3	—	38	0.875	3
23.1	12.4	12.8	—	36	0.88	18
32	27.2	9.9	—	30.6	0.885	1
40.7	38.1	7.7	—	23.1	0.895	1.6
50.9	47.4	8	6	19.1	0.902	1
49.5	47.4	6.3	2.3	19.5	0.902	3
48.8	45.9	7.9	10.5	19.3	0.902	3
45.5	41.2	9.8	14.2	19.7	0.902	30
59.1	57.4	4.9	1	13.8	0.91	0.5
58.7	57.3	4.3	0.6	14.3	0.91	1
56	54.7	5.5	1.2	15.1	0.91	3.5
59.4	56.7	6.5	1.8	14.8	0.911	6
56.6	52.1	8.7	3.7	15.1	0.913	30
57	50.3	9.3	4.6	15.2	0.913	30
64.8	63.6	4.2	0.5	10.8	0.915	1
						2
78.7	78.1	4.1	0.5	2.5	0.935	

T_c is the peak crystallization temperature, T_w is the weight-average crystallization temperature, Sigma and R are parameters defining the broadness of the CCD as per equations 2.3 and 2.4

Fig. 2.29 CRYSTAF calibration curve based on homogeneous EO copolymers (reprinted from [103] with permission of J. Wiley & Sons)



$$T_w = \frac{\sum c_i \cdot T_i}{\sum c_i} \quad T_n = \frac{\sum c_i}{\sum c_i / T_i} \quad (2.3)$$

$$\sigma = \sqrt{\frac{\sum c_i (T_i^2 - T_w^2)}{\sum c_i}} \quad R = \left(\frac{T_w}{T_n} - 1 \right) \cdot 100 \quad (2.4)$$

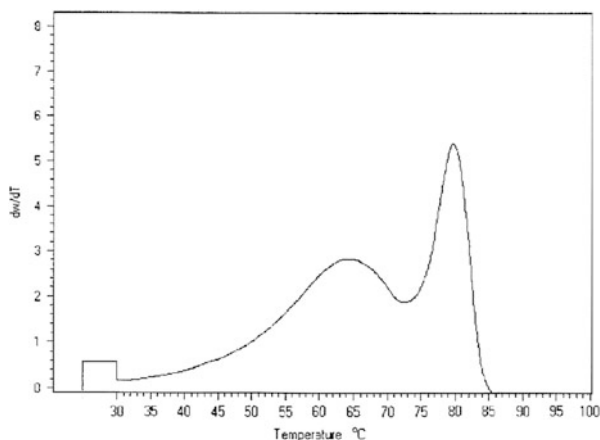
2.2.1.5 Discussion and Evaluation

As is seen in Table 2.5, most of the copolymer samples exhibit narrow CCDs. This makes them good candidates as calibration standards for CRYSTAF and TREF. Such calibrations are required to relate the crystallization (or elution) temperature to the comonomer content. For such copolymers, it is assumed that they are strictly linear and do not have long chain branches. Based on comonomer contents, analysed by ^{13}C -NMR spectroscopy, a calibration plot of crystallization temperature vs. wt% octene can be constructed. As is seen in Fig. 2.29, a straight line is obtained that indicates (1) a good correlation with the equilibrium theory of Flory, and (2) the crystallization temperature is practically independent of molar mass (see melt index in Table 2.5).

The present calibration curve can be used to quantify the CCD of EO copolymers irrespective of their origin and production process. As an example, the CRYSTAF analysis of a heterogeneous ZN LLDPE material is shown in Fig. 2.30.

In contrast to the CCDs in Fig. 2.28, this polymer shows a broad CCD, with a component that crystallizes at high temperature (HDPE), a range of components that crystallize between 70 °C and 30 °C (crystallizable EO copolymers with increasing EO contents) and non-crystallizable components (EO copolymers with a high octene content). In CRYSTAF, the non-crystallizable (soluble) components are presented as a rectangular concentration profile. The temperature axis as shown in Fig. 2.30 can be converted into a 'wt% octene' axis using the calibration curve in Fig. 2.29.

Fig. 2.30 CRYSTAF analysis of a heterogeneous ZN LLDPE (reprinted from [103] with permission of J. Wiley & Sons)



2.2.2 Analysis of Blends of Polyethylene and Polypropylene [104]

Polymer blends are very important commercial materials that combine useful properties of different polymers in a single product without involving any chemical reaction. The approach provides a good alternative to developing new tailor-made polymeric structures. The blending is a particularly feasible and commercially viable approach for polyolefins. Polyolefin blends ranging from blends of homopolymers to blends of homo- and copolymers are commercially available to achieve some selected application properties.

There are no universal methods available for the identification and quantitative determination of blend components and this is a demanding analytical challenge. The most widely used techniques for this purpose are spectroscopic techniques such as FTIR and NMR. These are averaging techniques; they are unable to differentiate between mixtures of two homopolymers and a copolymer with similar chemical compositions. Therefore, a separation step is often required prior to spectroscopic analysis for proper characterization of these complex polymers. This is particularly challenging for polyolefin blends because they dissolve only at high temperatures.

The most widely used method to separate polymer blends is the separation according to molar mass by SEC. This is only a viable method if the blend components have sufficiently different molar masses. DSC or TREF provide other approaches for compositional analysis by determining the melting and crystallization behaviour, respectively. DSC is advantageous in the analysis of blends due to the required equipment being simple and widely available. Another advantage of using DSC for blend analysis is that very small amounts of components can be detected. However, quantitative analysis by DSC is problematic. Thermal history problems that must be considered in DSC are eliminated in TREF as crystallization takes place from dilute solutions. TREF has been successfully used for the separation of copolymers and polymer blends [16, 105–109]. The separation and quantification of different components of the blends of HDPE, LDPE, LLDPE

and PP are possible. The long analysis times and the inefficiency in separating PE and EP copolymers are the only limitations of TREF.

2.2.2.1 Aim

In the present application, the capabilities of CRYSTAF for the fractionation of polyolefin blends shall be explored. CRYSTAF is faster than TREF and is based on a single crystallization step of the blend components out of the solution. The detection limit of each component shall be determined and compared to DSC for investigation of blends of metallocene-catalysed PE and PP. The successful separation and quantification of blends of commercial HDPE, LDPE and PP shall be demonstrated. Finally, the analysis of recycled polyolefins by CRYSTAF shall be discussed. It shall be demonstrated that CRYSTAF can be the workhorse of the polyolefin industry for routine analysis of complex polyolefin blends to obtain direct quantitative results.

2.2.2.2 Materials

- *Polymers.* Laboratory products of metallocene-catalysed PE and PP, and commercial HDPE, LDPE and PP.

2.2.2.3 Equipment

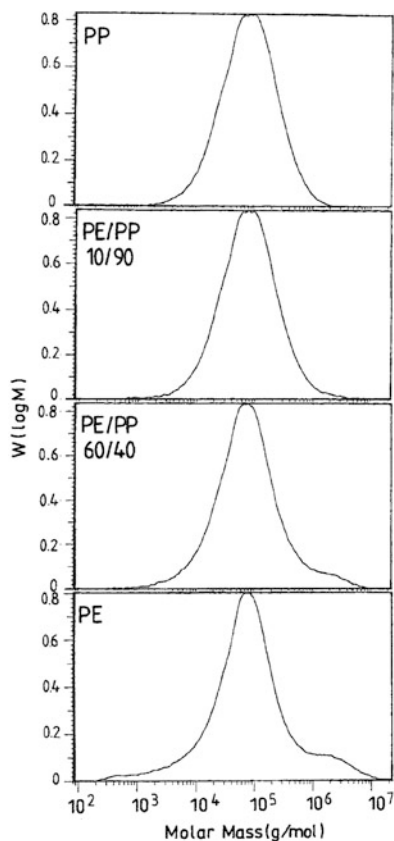
- *CRYSTAF system.* CRYSTAF instrument model 200 (Polymer Char, Valencia, Spain).
- *Detector.* Built-in dual wavelength IR detector with heated flow-through micro cell at 150 °C.
- *Solvent.* TCB.
- *Crystallization protocol.* Crystallization between 100 °C and 30 °C, at a rate of 0.1 °C/min.
- *Sample concentration.* 30 mg in 30 mL TCB.
- *DSC.* Perkin-Elmer DSC 7 (Perkin-Elmer, Waltham, USA), heating and cooling rates of 10 °C/min were applied. DSC curves of the second heating cycle were used for analysis.
- *SEC.* Waters 150 HT-SEC apparatus (Waters Inc., Milford, USA) equipped with a differential refractometer, oven temperature 145 °C, mobile phase TCB, column set: Styragel 500 Å + HT3 + HT4 + HT5 + HT6, flow rate 1 mL/min.

2.2.2.4 Preparatory Investigations

Blends of metallocene-catalysed PE and PP were analysed by SEC and DSC as a first step. The molar masses of the blend components (PE 342 kg/mol and PP 143 kg/mol) are not very different. Therefore, SEC was not the technique of choice for this separation. The MMDs for PE/PP blends of varying compositions are shown in Fig. 2.31.

DSC separates with regard to melting or crystallization temperatures. PE melts at 132 °C while PP melts at 147 °C. The difference is sufficiently large to obtain well resolved melting peaks. As long as the concentration of PP exceeds 20 %, both components can be easily identified; see Fig. 2.32. For blends containing low

Fig. 2.31 SEC separation of metallocene-catalysed PE and PP and a PE/PP blend (reprinted from [104] with permission of Wiley-VCH)



amounts of PP, it is difficult to detect the PP peak in a routine experiment. The melt enthalpy is a function of crystallinity and thermal history of the sample; therefore, quantitative information on blend composition is rather difficult to obtain, unless further information on the samples is obtained by additional measurements.

2.2.2.5 CRYSTAF Fractionations

The CRYSTAF results of a variety of PE/PP blends are presented in Fig. 2.33. The crystallization temperatures of the blend components are clearly different. PE crystallizes at higher temperature (86.3 °C) compared to PP (70.5 °C). Narrow and well resolved crystallization peaks are obtained for both PE and PP. A true concentration profile is obtained directly, unlike with DSC. Therefore, the relative concentrations of the components can be calculated directly from the experimental results without further assumptions.

In contrast to DSC, very low concentrations of the blend components can be detected, as seen in Fig. 2.33. The detection limits for both components are very low (5 wt% for PP and 2–3 wt% for PE). As can be seen in Fig. 2.34, the experimental

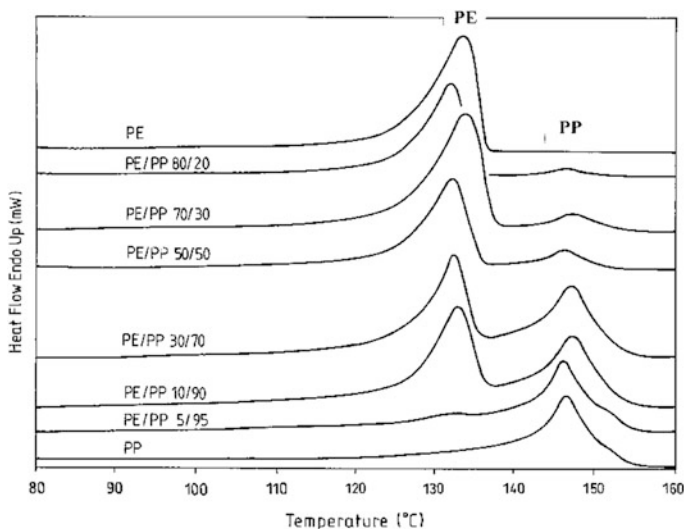


Fig. 2.32 DSC analysis of metallocene-catalysed PE and PP and PE/PP blends (reprinted from [104] with permission of Wiley-VCH)

blend composition as calculated by CRYSTAF agrees quite well with the nominal composition of the samples over the entire range of compositions.

2.2.2.6 Discussion and Evaluation

ZN-catalysed polyolefins and their blends still dominate industrial applications. DSC is not capable of analysing different blends of HDPE and LDPE because the melting temperatures of both components are quite similar and the DSC peaks are rather broad. The CRYSTAF analysis revealed excellent separation of blends with varying compositions of HDPE (Lupolen 5261Z) and LDPE (Lupolen 1800H), as can be seen in Fig. 2.35. The sharp crystalline peak for HDPE appeared at 88.0 °C and a small fraction of less than 5 % crystallized at lower temperature suggesting small amounts of less crystalline PE. At an even lower temperature of 59.1 °C, a broad crystallization peak for LLDPE is obtained.

The CRYSTAF analysis revealed well separated crystallization peaks for blends of HDPE and LDPE that can be quantified easily in the composition range of HDPE/LDPE 90/10 to 10/90. The lower detection limit for HDPE is less than 4 wt% in this case. The detection limit for LDPE is higher because HDPE itself contains some less crystalline material. The lower detection limit for LDPE in the present case is 10 wt%. Figure 2.36 demonstrates the comparison of CRYSTAF results with the nominal composition of the sample. Excellent agreement is found over the entire range of compositions.

An increasingly important topic is the characterization of waste plastics or materials resulting from recycling processes. Recycled plastics frequently contain several diverse components and these must be analysed with regard to their PP,

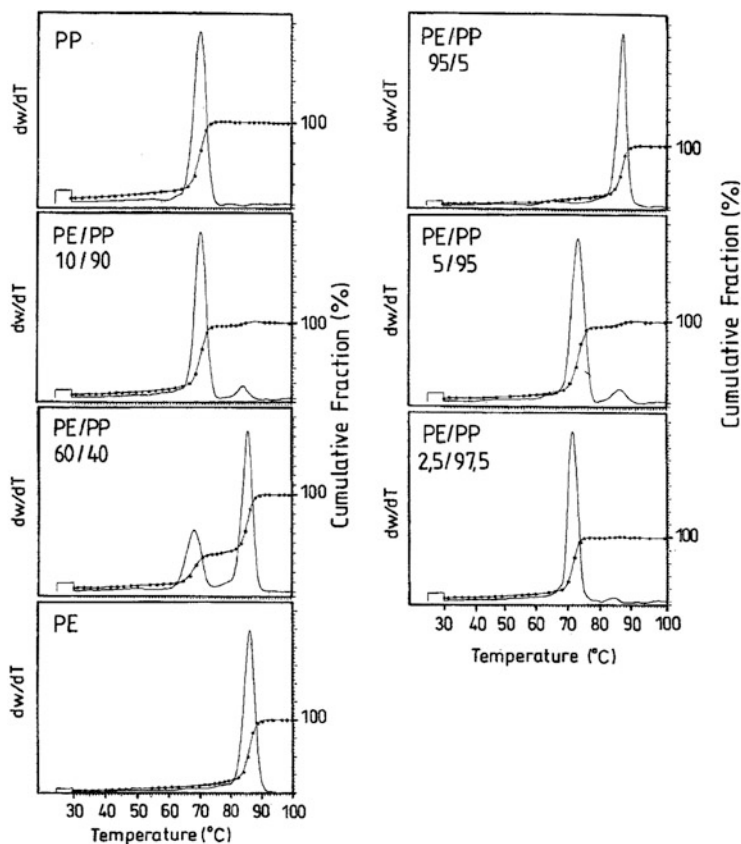


Fig. 2.33 CRYSTAF analysis of metallocene-catalysed PE and PP and PE/PP blends (reprinted from [104] with permission of Wiley-VCH)

HDPE and LDPE contents. DSC can be used to determine PP in such materials but as explained earlier the determination of the ratio of HDPE and LDPE in such materials by DSC is rather difficult. CRYSTAF is the method of choice for the analysis of such materials and three components can be easily identified and quantified. Figure 2.37 displays a comparison of CRYSTAF and DSC results of a waste plastic material. The three components, namely HDPE, PP and LDPE, can be recognized by their crystallization peaks and the peak areas directly reveal the concentration of the components. The crystallization peaks of the three components show slight overlapping. Nonetheless, the relative amounts of the three components can be determined to be about 40/27/33 wt%.

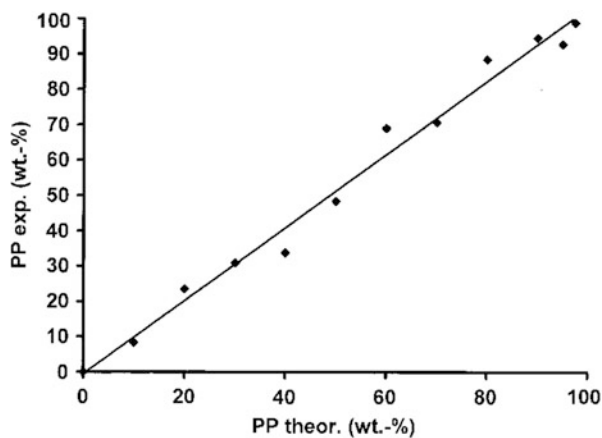


Fig. 2.34 Comparison of experimental and nominal PP content in PE/PP blends (reprinted from [104] with permission of Wiley-VCH)

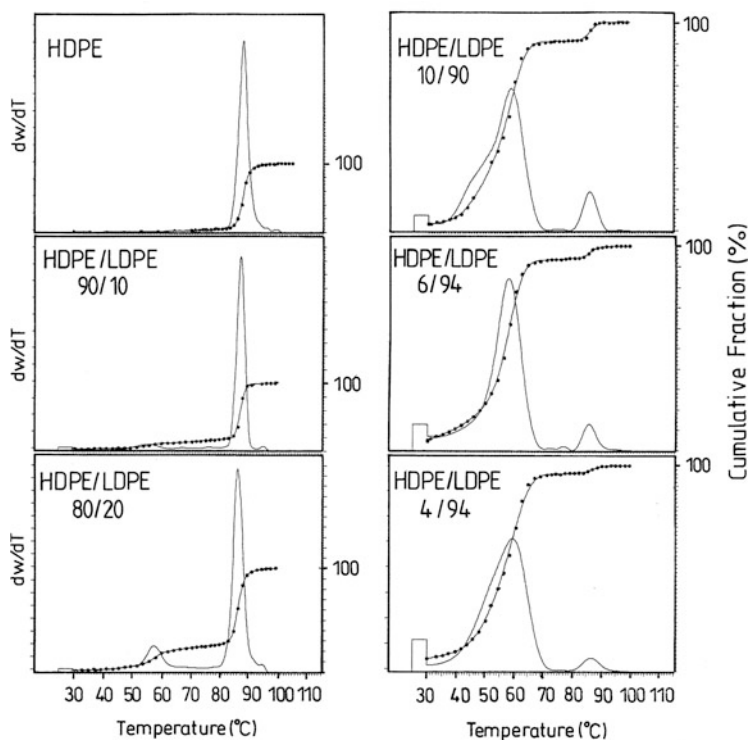


Fig. 2.35 CRYSTAF analysis of HDPE/LDPE blends (reprinted from [104] with permission of Wiley-VCH)

Fig. 2.36 Comparison of experimental and nominal HDPE content in HDPE/LDPE blends (reprinted from [104] with permission of Wiley-VCH)

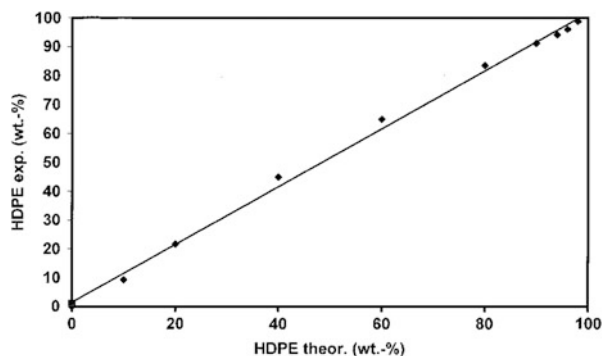
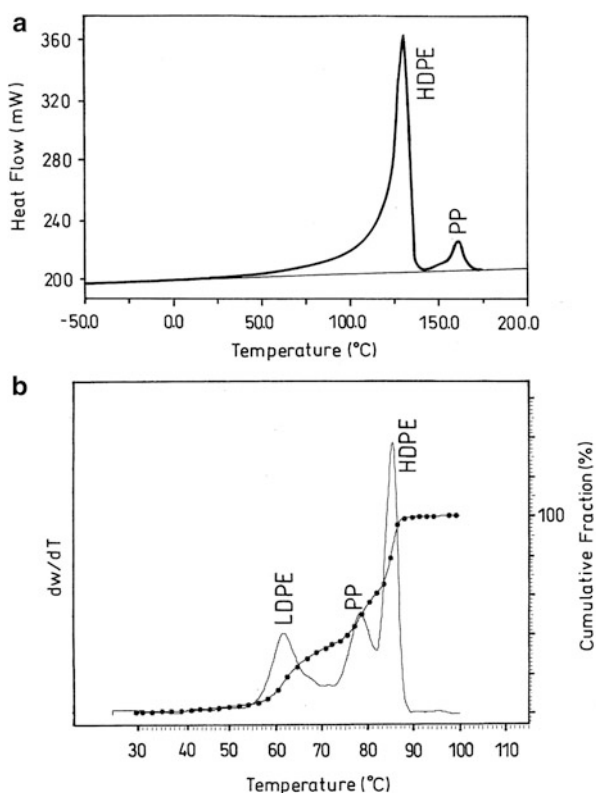


Fig. 2.37 Comparison of DSC (a) and CRYSTAF (b) of a waste plastic sample containing HDPE, LDPE and PP (reprinted from [104] with permission of Wiley-VCH)



2.2.3 Analysis of Copolymers of Propylene and Higher α -Olefins [110]

Random copolymers of ethylene and higher α -olefins are important commercial materials that are typically classified as LLDPE. In contrast to the technical

applications of LLDPE, random copolymers of propylene and higher α -olefins are less frequently investigated and used. Most of the work that has been done over the years has dealt with copolymers of propylene and ethylene, one example being IPCs; see, e.g. Sect. 2.1.2.

As has been discussed earlier (Sect. 2.2.1) there is a direct correlation between the crystallization temperature and the copolymer composition. This has been documented for LLDPEs with butene, hexene or octene as comonomers. The crystallization behaviour of random copolymers of ethylene was reviewed by Alamo and Mandelkern [111]. According to them, a linear relationship describes the melting temperature of ethylene/higher α -olefin copolymers versus the comonomer content up to 4 mol%. The type of comonomer has no effect on the melting temperature. In agreement with these findings, the CRYSTAF and TREF analysis of narrow LLDPE fractions revealed a linear correlation between crystallization temperature and comonomer content [8, 16]. The CRYSTAF and TREF apparatus were calibrated by the crystallization temperature of single-site ethylene-1-octene (EO) copolymers and the calibration was subsequently used for the analysis of broadly distributed industrial LLDPE samples [103].

2.2.3.1 Aim

There are numerous studies on the melting and crystallization behaviour of ethylene- α -olefin copolymers. However, copolymers based on propylene have not received much attention. In the present study, these copolymers shall be investigated by DSC and CRYSTAF. The influence of the comonomer shall be investigated for propylene copolymers with 1-octene, 1-decene, 1-tetradecene and 1-octadecene.

2.2.3.2 Materials

- *Polymers.* The copolymerizations were conducted according to the procedure described in [110]. The catalyst was $(\text{CH}_3)_2\text{Si}(2\text{-methylbenz[e]indenyl})\text{ZrCl}_2$. The copolymer compositions are summarized in Table 2.6. The molar masses were determined by SEC.

2.2.3.3 Equipment

- *CRYSTAF system.* CRYSTAF instrument model 200 (Polymer Char, Valencia, Spain).
- *Detector.* Built-in dual wavelength IR detector with heated flow-through micro cell at 150 °C.
- *Solvent.* TCB.
- *Crystallization protocol.* Crystallization between 100 °C and 30 °C at a rate of 0.1 °C/min.
- *Sample concentration.* 20 mg in 30 mL TCB.
- *DSC.* Pyris 1 (Perkin-Elmer, Waltham, USA). Samples were cooled to -50 °C and then heated to 180 °C. From 180 °C, samples were again cooled to -50 °C. The cooling rate was kept at 10 °C/min. T_c was determined from the maximum

Table 2.6 Comonomer content, melting temperature T_m , crystallization temperature from melt T_c (melt) (DSC), crystallization temperature from solution T_c (sol) (CRYSTAF), molar masses and molar mass dispersities (adopted from [110] with permission of Wiley-VCH)

Sample	Comonomer	Comonomer (mol-%)	T_m (°C)	T_c (melt) (°C)	T_c (sol) (°C)	\bar{M}_w (g/mol)	\bar{M}_w/\bar{M}_n
3.1	None	0	149.0	112.4	75.4	460,700	2.80
8.8	1-Octene	0.47	141.1	101.6	66.4	600,200	2.34
8.5		0.55	140.1	99.0	62.9	539,700	2.47
8.7		0.57	142.1	99.1	63.7	421,500	2.19
8.4		0.86	137.1	90.0	58.9	456,900	2.25
8.6		1.27	125.7	77.4	50.8	156,200	3.11
8.2		2.89	108.2	66.7	34.9	303,800	1.94
8.9		3.43	106.4	64.8	30	304,500	2.15
10.6	1-Decene	0.42	145.9	96.4	63.4	466,200	2.30
10.8		0.47	144.4	98.6	65.9	448,800	2.64
10.7		0.72	140.6	95.2	58.3	428,300	2.24
10.5		0.78	145.9	100.9	63.7	272,100	2.28
10.4		1.07	138.2	89.7	57.1	427,700	2.21
10.3		1.39	128.1	84.7	49	372,700	2.39
10.2		2.31	115.4	67.0	38.7	297,400	2.10
10.9		2.39	111.9	70.1	30	346,800	2.05
14.8	1-Tetradecene	0.26	144.1	98.2	65.8	282,700	2.29
14.7		0.5	143.2	96.2	59.4	240,700	2.14
14.4		0.63	142.3	93.2	57.7	572,300	2.23
14.5		0.68	136.3	91.9	55.2	553,500	2.54
14.6		0.77	144.3	94.4	60.1	369,700	2.35
14.3		0.89	130.8	89.7	51.5	639,200	2.51
14.1		1.05	126.5	81.7	47	413,200	2.15
14.10		2.33	114.5	66.9	34.5	415,500	2.15
14.2		2.76	108.4	64.3	30	395,100	2.31
18.6	1-Octadecene	0.47	143.3	101.5	61.4	279,700	2.21
18.8		0.51	142.1	106.3	62.9	223,700	2.44
18.4		0.66	139.1	94.3	59	764,300	2.20
18.5		0.81	137.8	88.9	55.5	486,200	2.27
18.10		1.09	131.4	86.9	50.6	494,600	2.05
18.9		1.49	127.4	86.4	45	307,700	2.02
18.11		1.89	122.8	81.5	38.7	442,000	1.99
18.2		2.04	124.5	–	41.2	380,500	1.95

of the exotherm in the cooling cycle. While the sample was heated from $-50\text{ }^{\circ}\text{C}$ to $180\text{ }^{\circ}\text{C}$ at a heating rate of $10\text{ }^{\circ}\text{C}/\text{min}$, the melting endotherm was recorded. T_m was determined from the peak maximum of the second heating cycle.

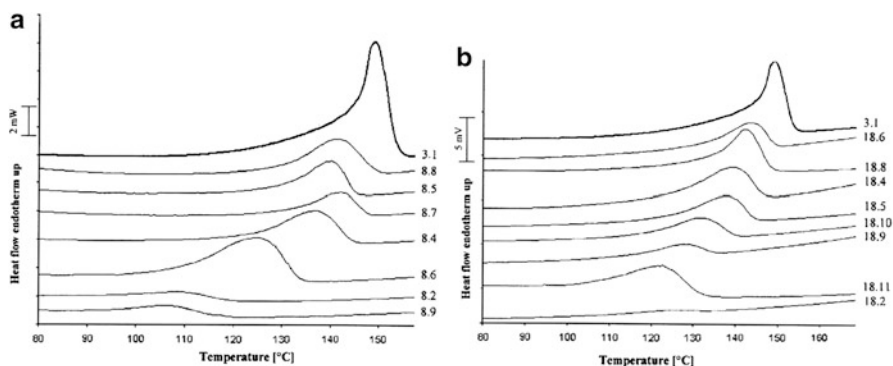


Fig. 2.38 DSC analysis of metalloocene-catalysed propylene- α -olefin copolymers, second heating cycle, comonomer 1-octene (a), comonomer 1-octadecene (b) (reprinted from [110] with permission of Wiley-VCH)

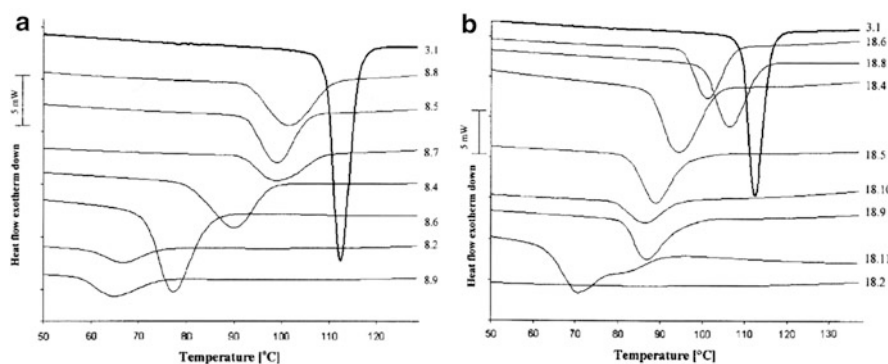


Fig. 2.39 DSC analysis of metalloocene-catalysed propylene- α -olefin copolymers, first cooling cycle, comonomer 1-octene (a), comonomer 1-octadecene (b) (reprinted from [110] with permission of Wiley-VCH)

2.2.3.4 CRYSTAF and DSC Measurements

The copolymers were prepared by solution polymerization using a single-site catalyst. Conversions were kept to below 50 %. Comonomer contents were restricted to an upper limit of 3.5 mol%. ^{13}C -NMR spectroscopy was used to determine the amount of comonomer incorporated into the copolymer. All copolymers had high molar masses and low molar mass dispersities. The analytical data for the copolymers are summarized in Table 2.6.

The discussion of the thermal behaviour of the copolymers focuses on the 1-octene and the 1-octadecene copolymers as the two extremes. Their DSC heating and cooling curves are summarized in Figs. 2.38 and 2.39. The DSC curves are positioned according to the amount of comonomer incorporated. The peak melting temperature, T_m , was recorded from the maximum of the endotherm and the crystallization temperature from melt, T_c (melt), was recorded from the maximum

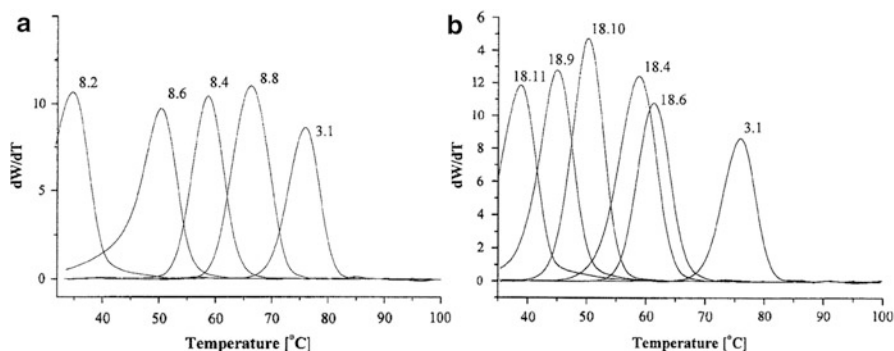


Fig. 2.40 CRYSTAF analysis of metallocene-catalysed propylene- α -olefin copolymers, comonomer 1-octene (a), comonomer 1-octadecene (b) (reprinted from [110] with permission of Wiley-VCH)

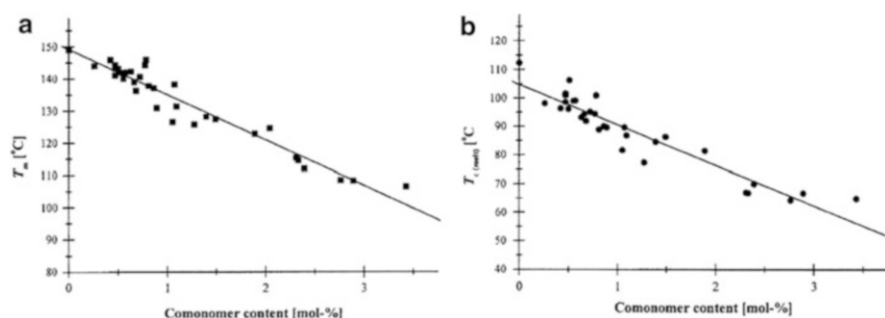


Fig. 2.41 Melting temperature T_m (a) and crystallization temperature T_c (melt) (b) as a function of copolymer composition, determined by DSC (reprinted from [110] with permission of Wiley-VCH)

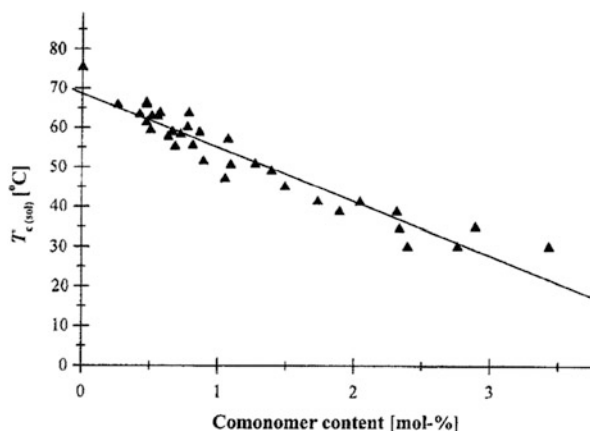
of the exotherm. The melting temperatures obtained during the second heating cycle were considered in order to ensure identical thermal histories of the investigated copolymers.

The CRYSTAF analysis of the 1-octene and the 1-octadecene copolymers is shown in Fig. 2.40. Copolymers with higher comonomer contents (e.g. entries 8.2 and 18.11) partially crystallize at temperatures lower than 30 °C. This is not relevant in the current study because only the peak maximum temperatures are used in the discussion.

2.2.3.5 Discussion and Evaluation

The dependence of the melting temperature determined by DSC follows the expected linear relationship according to the Flory–Huggins theory. As expected, the nature of the comonomer does not influence the melting point depression. Figure 2.41a demonstrates the melting points of all synthesized propylene/ α -olefin

Fig. 2.42 Crystallization temperature T_c (sol) as a function of copolymer composition, determined by CRYSTAF (reprinted from [110] with permission of Wiley-VCH)



copolymers as a function of the comonomer content. It can be clearly seen that melting point depression is independent of the type of comonomer. The molar mass of the copolymers was not treated as an independent variable as the molar masses were sufficiently high not to be an influencing factor.

For the investigation of the crystallization behaviour, a constant cooling rate was applied to the crystallization from the melt (DSC) and from dilute solution (CRYSTAF). It is well accepted from TREF studies of polyolefins that above a molar mass of 15 kg/mol the crystallization behaviour is independent of the chain length [5]. The molar masses of propylene/higher α -olefin copolymers in the current study are well above this threshold; therefore crystallization behaviour is presumed to be independent of molar mass. DSC measurements provided T_c (melt), and are plotted against comonomer content of all copolymers; see Fig. 2.41b. The decrease of T_c (melt) with increasing comonomer content seems to be independent of the nature of the respective comonomers. The explanation given earlier for depression in the melting point being independent of the comonomer type is valid in this case too. After plotting the peak crystallization temperature from solution, T_c (sol) obtained by CRYSTAF versus the amount of comonomer incorporated, a straight line relationship is found. Similar to T_m and T_c (melt), T_c (sol) is independent of the nature of the comonomer; see Fig. 2.42.

All the illustrated regression curves summarized in Fig. 2.43 follow the linear relationship $y = -Ax + B$. The degree of the temperature depression for the melting process or the crystallization from melt as well as from dilute solution is described by coefficient A that is constant within experimental error, as can be seen in Table 2.7. The parallel lines for the regression curves in Fig. 2.43 manifest this fact. However, the crystallization from dilute solution occurs at significantly lower temperature than the crystallization process from melt.

It is important to mention here that the comonomers used in the current study had sufficiently bulky side chains to be excluded from all crystalline structures. The effect of lower α -olefins might not be the same. The copolymers composed of

Fig. 2.43 T_m , T_c (melt) and T_c (sol) as a function of copolymer composition (reprinted from [110] with permission of Wiley-VCH)

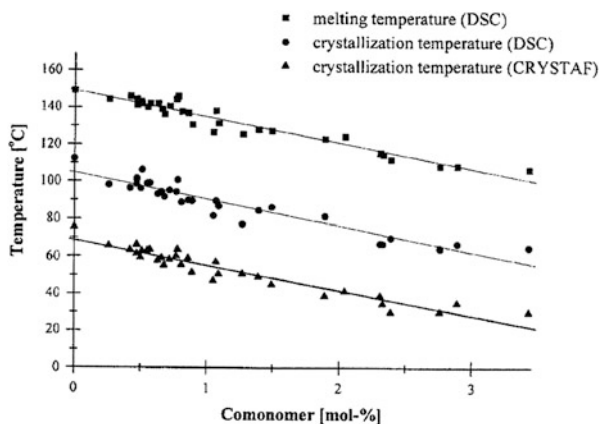


Table 2.7 Regression curves calculated using least square regression analysis assuming the function $y = -Ax + B$ (y = melting/crystallization temperature in °C, x = comonomer content in mol%)

	A (°C/mol%)	B (°C)	R^2
Melting (DSC)	14.1 ± 0.7	149.1 ± 1.0	0.93
Crystallization (DSC)	14.2 ± 0.9	104.7 ± 1.3	0.88
Crystallization (CRYSTAF)	13.7 ± 0.8	68.6 ± 1.1	0.91

The best fit was obtained with the constants A and B . The coefficient of fit was R^2 (adopted from [110] with permission of Wiley-VCH)

propylene-1-butene showed crystalline behaviour over the entire range of compositions, indicating the co-crystallization of 1-butene with propylene [112].

2.3 Crystallization Elution Fractionation

A further refinement of crystallization-based fractionation techniques was recently introduced by Monrabal et al. with the development of crystallization elution fractionation (CEF) [113]. Combining the advantages of TREF and CRYSTAF, the aim of CEF is to improve the separation and to decrease the fractionation time. This is achieved by using dynamic crystallization as the first step of the process. In TREF, crystallization takes place in the column statically and all polymer fractions crystallize on the solid support at the same location, forming onion-like crystalline layers; see Fig. 2.1. In CEF, crystallization of the different polymer fractions takes place at different locations in the column. This is achieved by applying a small flow of the solvent in the column.

Figure 2.44 demonstrates the differences between normal TREF, dynamic crystallization and CEF. Figure 2.44a depicts the typical TREF process, where the first step is sample loading at high temperature, followed by stepwise crystallization of the polymer components by crystallizability. The same sample loading is the first

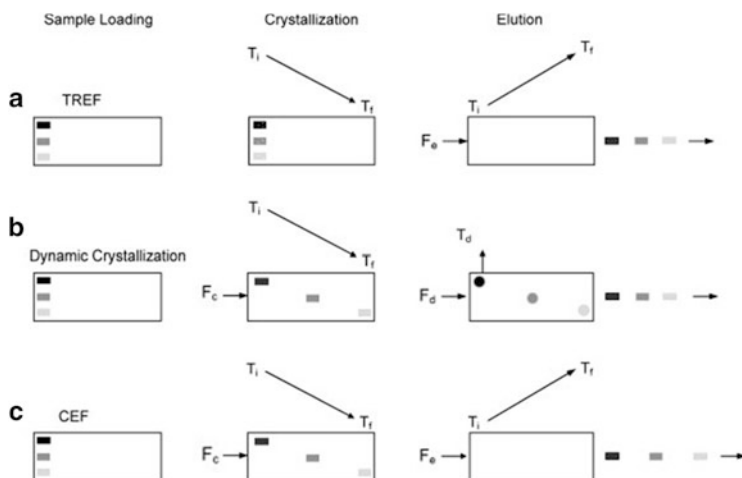


Fig. 2.44 Separation diagram by crystallizability. TREF (a), dynamic crystallization (b), CEF (c) (reprinted from [114] with permission of Wiley-VCH).

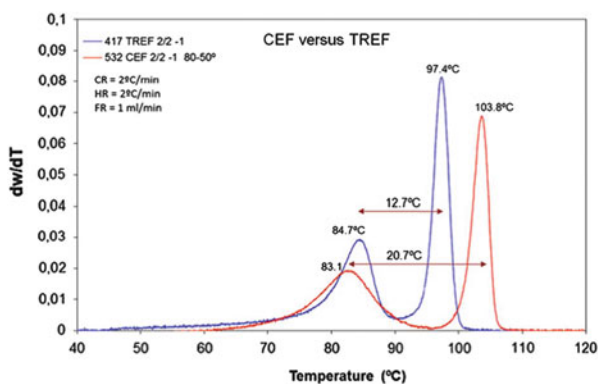


Fig. 2.45 Separation of two metallocene-type resins of very similar densities by TREF and CEF, cooling rate 2 °C/min, CEF crystallization flow 0.4 mL/min, elution flow 1 mL/min (reprinted from [9] with permission of Springer Science + Business Media)

step in dynamic crystallization where a continuous solvent flow is maintained through the column during the cooling process; see Fig. 2.44b. The polymer components that reach their crystallization temperatures will segregate and anchor on the support while other components in solution move along until they reach their crystallization temperatures. The physical separation of the polymer components is achieved with regard to crystallizability within the column in the crystallization cycle. The key to improving separation during the crystallization step is the flow rate. After the completion of crystallization, the solvent flow is stopped and dissolution of the polymer components is achieved by heating the column to higher

temperatures. To elute all different fractions, the solvent flow is started again at an appropriate rate.

The advantages of the two processes explained in Fig. 2.44a, b are combined in CEF. The sample loading step is the first step. It is the same for all three methods. The crystallization with a continuous flow through the column enhances the physical separation according to crystallinity during this step and this dynamic crystallization is combined with the typical TREF elution cycle as a next step; see Fig. 2.44c. The set-up resulted in enhanced resolution in a shorter time frame.

CEF has been shown to provide reproducible and very fast analyses of the compositional distribution of complex polyolefins, one application being in high-throughput experimentation [114]. Analysis times of less than 30 min could be achieved. The gain in separation from TREF to CEF is presented in Fig. 2.45 for a blend of two metallocene-type resins [9]. The crystallization peaks of the two components are separated by 20.7 °C for CEF compared to only 12.7 °C for TREF.

2.3.1 Analysis of Complex Polyolefins by CEF [113]

As mentioned earlier, CEF is faster than TREF and CRYSTAF, and significantly improved fractionations are obtained. This makes CEF an interesting alternative to the more conventional polyolefin fractionation techniques. CEF experiments can be conducted in a standard TREF instrument as they only require a typical tunable column oven and a HPLC pump to deliver the solvent flow. Similar to TREF, a range of different detectors can be used to monitor concentration, chemical composition and molar mass.

2.3.1.1 Aim

In the present application, a range of different complex polyolefins shall be fractionated. The experimental approach of CEF shall be described and the quality of fractionations obtained shall be discussed.

2.3.1.2 Materials

- *Polymers.* Metallocene-type resins with densities of 0.902 g/mL and 0.937 g/mL, Elite™ resin of Dow Chemical, LLDPE

2.3.1.3 Equipment

- *CEF.* CEF Instrument (Polymer Char, Valencia, Spain); see Fig. 2.46.
- *Detectors.* Dual wavelength IR detector, dual capillary viscometer.
- *Solvent.* ODCB.
- *Crystallization and elution protocol.* As described in the text.

2.3.1.4 CEF Measurements and Discussion

The fractionation of a typical complex polyolefin, Elite™ from Dow Chemical, is shown in Fig. 2.47. This fractionation was accomplished in only 23 min using very fast crystallization and heating rates (10 °C/min for both). Nevertheless, excellent

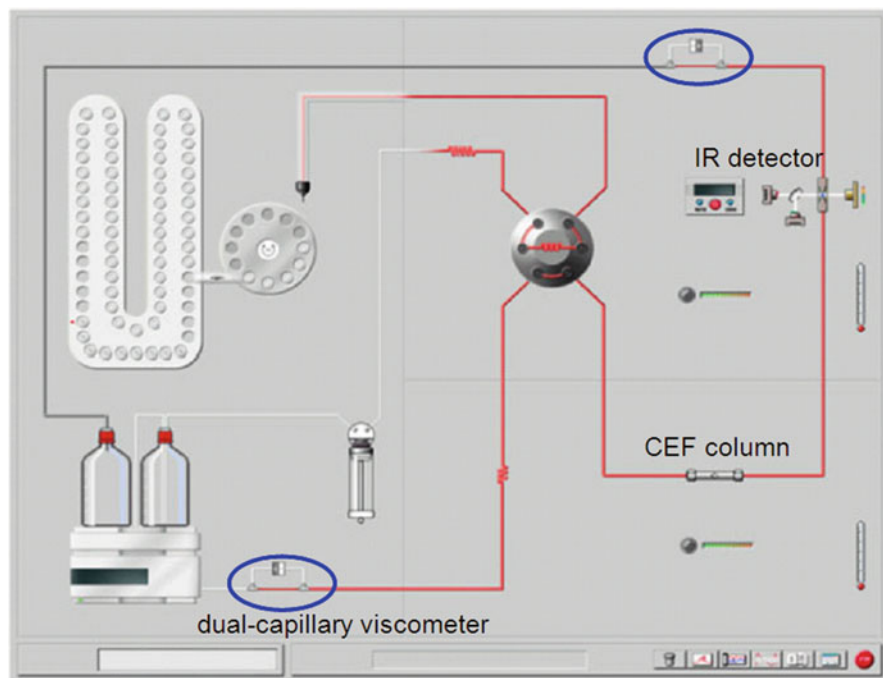


Fig. 2.46 Schematic diagram of instrument combining TREF, dynamic crystallization and CEF (reprinted from [113] with permission of Wiley-VCH)

separation into the different components is achieved. The reproducibility of multiple fractionations is very good, as can be seen in Fig. 2.48 for the same resin. This makes CEF a preferred choice for conducting fast and repeated fractionations, for example, of an unknown material. Sufficiently large fractions can be accumulated that allow further analyses, e.g. by NMR spectroscopy.

The separation of a LLDPE by multidetector CEF is presented in Fig. 2.49. The dual wavelength IR detector provides the concentration reading while the ratio of the CH_2 and CH_3 signals from the IR detector provides the copolymer composition ($\text{CH}_3/1,000\text{C}$). The molar mass is obtained from the online capillary viscometer reading that provides the intrinsic viscosity distribution.

To summarize, CEF is an interesting alternative method to TREF and CRYSTAF and can be performed in a simplified TREF instrument. Better information can be obtained in a fraction of the time that is required for TREF or CRYSTAF.

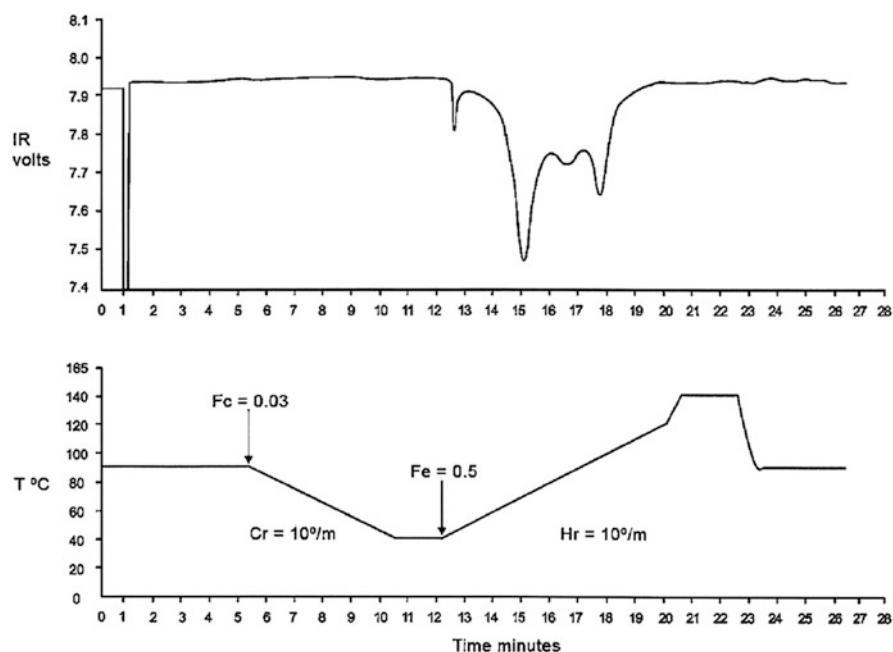


Fig. 2.47 CEF analysis of Elite™ resin: *top diagram* shows the IR concentration reading, *bottom diagram* shows the crystallization and elution temperature profiles (reprinted from [113] with permission of Wiley-VCH)

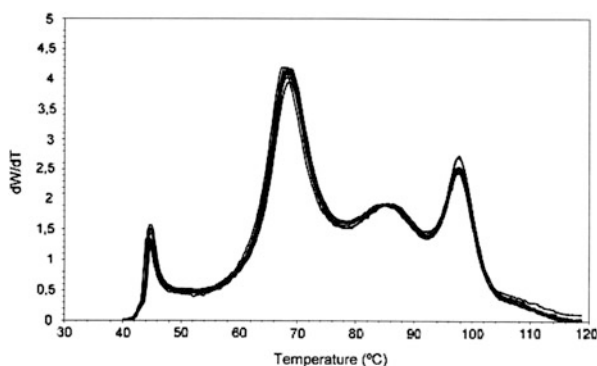


Fig. 2.48 Multiple CEF analyses (10 times) of Elite™ resin: crystallization rate $5^\circ C/min$, heating rate $10^\circ C/min$, elution flow rate 0.5 mL/min (reprinted from [113] with permission of Wiley-VCH)

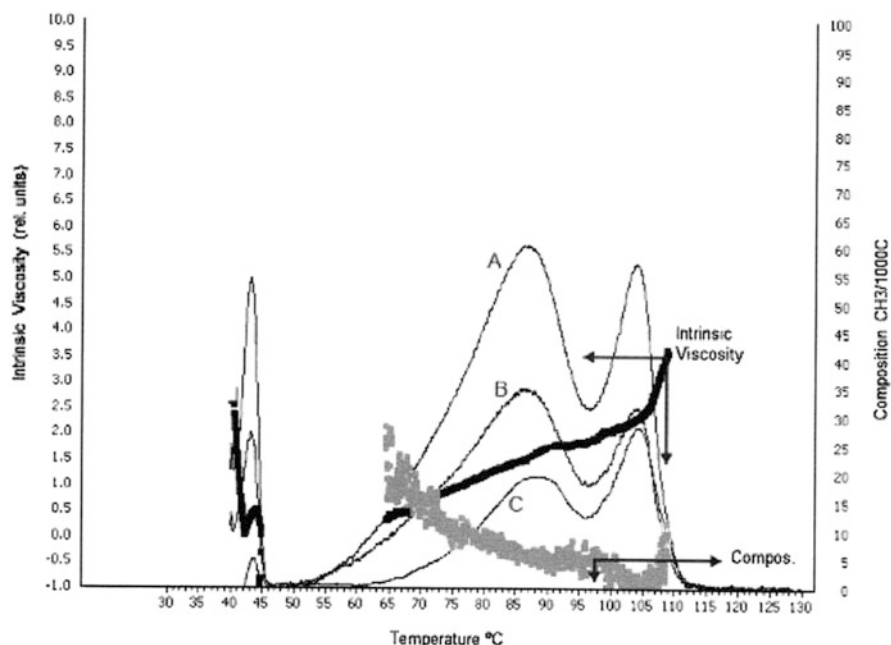


Fig. 2.49 CEF analysis of LLDPE: A—concentration, B—composition, C—intrinsic viscosity (reprinted from [113] with permission of Wiley-VCH)

References

1. Wild L, Ryle T, Knobeloch D, Peat IR (1982) *J Polym Sci Polym Phys Ed* 20:441
2. Wild L, Blatz C (1993) In: Chung T (ed) *New advances in polyolefins*. Plenum, New York, NY
3. Alamo R, Mandelkern L (1989) *Macromolecules* 22:1273
4. Monrabal B (1994) *J Appl Polym Sci* 52:491
5. Desreux V, Spiegels ML (1950) *Bull Soc Chim Belg* 59:476
6. Soares JBP, Hamielec AE (1999) In: Petrick RA (ed) *Modern techniques for polymer characterization*. Wiley, New York, NY, p 1
7. Anatawaraskul S, Soares JBP, Wood-Adams PM (2005) *Adv Polym Sci* 182:1
8. Monrabal B (2000) Temperature rising elution fractionation and crystallization analysis fractionation. In: Meyers RA (ed) *Encyclopedia of analytical chemistry*. Wiley, Chichester, p 9074
9. Monrabal B (2013) *Adv Polym Sci* 257:203
10. Pasch H, Malik MI, Macko T (2013) *Adv Polym Sci* 251:77
11. Flory PJ (1948) *Trans Farad Soc* 51:848
12. Flory PJ (1953) *Principles of polymer chemistry*. Cornell University Press, Ithaca, NY
13. Wunderlich B (1980) *Macromolecular physics*, vol 3. Academic, New York, NY
14. Huggins ML, Okamoto H (1967) Chapter A: Theoretical considerations. In: Cantow MJ (ed) *Polymer fractionation*. Academic, New York, NY
15. Mueller A, Arnal L (2005) *Progr Polym Sci* 30:559

16. Wild L (1991) *Adv Polym Sci* 98:1
17. Hazlitt LG (1990) *J Appl Polym Sci Appl Polym Symp* 45:25
18. Kuhlman RL, Klosin J (2010) *Macromolecules* 43:7903
19. Cossoul E, Baverel L, Martigny E, Macko T, Boisson C, Boyron O (2013) *Macromol Symp* 330:42
20. Monrabal B (2007) Microstructure characterization of polyolefins. In: Abstracts: advances in polyolefins, 23–26 September 2007, ACS, Division of Polymer Chemistry, Santa Rosa
21. http://www.polymerchar.com/pdf/Gel_Permeation_Chromatograph_with_integrated_Infrared_Detector_IR5_MCT_for_Polyolefin_Analysis.pdf
22. Tomba JP, Carella JM, Pastor JM (2005) *J Polym Sci B Polym Phys* 43:3083
23. Hasan ATMK, Liu B, Terano M (2005) *Polym Bull* 54:22
24. Hasan ATMK, Fang Y, Liu B, Terano M (2010) *Polymer* 51:362
25. Liu Y, Bo S, Zhu Y, Zhang W (2005) *J Appl Polym Sci* 97:232
26. Zhang Y (2006) *J Appl Polym Sci* 99:845
27. Assumption HJ, Vermeulen JP, Jarrett WL, Mathias LJ, van Reenen AJ (2006) *Polymer* 47:67
28. Harding GW, van Reenen AJ (2006) *Macromol Chem Phys* 207:1680
29. Suzuki S, Nakamura Y, Hasan ATMK, Liu B, Terano M, Nakatani H (2005) *Polym Bull* 54:311
30. Gupta P, Wilkes GL, Sukhadia AM, Krishnaswamy RK, Lamborn MJ, Wharry SM, Tso CC, DesLauriers PJ, Mansfield T, Beyer FL (2005) *Polymer* 46:8819
31. Shan CLP, Hazlitt LG (2007) *Macromol Symp* 257:80
32. Albrecht A, Brüll R, Macko T, Sinha P, Pasch H (2008) *Macromol Chem Phys* 209:1909
33. Zhu H, Monrabal B, Han CC, Wang D (2008) *Macromolecules* 41:826
34. Amer I, van Reenen A (2009) *Macromol Symp* 282:33
35. Anantawaraskul S, Bongsontia W, Soares JBP (2009) *Macromol Symp* 282:167
36. Vadlamudi M, Subramanian G, Shanbhag S, Alamo RG, Varma-Nai M, Fiscus DM, Brown GM, Lu C, Ruff CJ (2009) *Macromol Symp* 282:1
37. de Goede E, Mallon P, Pasch H (2010) *Macromol Mater Eng* 295:366
38. Nakano M, Goto Y (1981) *J Appl Polym Sci* 26:4217
39. Aust N, Beytollahi-Amtmann I, Lederer K (1995) *Int J Polym Anal Char* 1:245
40. Faldi A, Soares JBP (2001) *Polymer* 42:3057
41. Li Pi Shan C, Gillespie D, Hazlitt L (2005) The Dow Company, Ecorep, Lyon
42. Gillespie D, Hazlitt L, Li Pi Shan C (2006) Proceedings of the 1st International Conference on Polyolefin Characterization (ICPC), Houston, October 2006
43. Yau WW (2007) *Macromol Symp* 257:29
44. Ortin A, Monrabal B, Sancho-Tello J (2007) *Macromol Symp* 257:13
45. http://www.polymerchar.com/pdf/Automated_Crossfractionation_Chromatography_CFC.pdf
46. Zhang Z (2009) *Macromol Symp* 282:111
47. http://www.chemsystems.com/about/cs/news/items/POPS09_Executive%20Report.cfm
48. DesLauriers PJ, Rohlfling DC, Hsieh ET (2002) *Polymer* 43:159
49. Fox JJ, Martin AE (1937) *Proc Royal Soc Lond* 162:419
50. Arriola DJ, Carnahan EM, Hustad PD, Kuhlman RL (2006) *Science* 321:714
51. Galli P, Haylock JC, Simonazzi T (1995) Manufacturing and properties of polypropylene copolymers. In: Karger-Kocsis J (ed) *Polypropylene: structure, blends and composites*, vol 3. Chapman & Hall, London
52. Mirabella F (1993) *Polymer* 34:1729
53. Usami T, Gotoh Y, Umemoto H, Takayama S (1993) *J Appl Polym Sci Appl Polym Symp* 52:145
54. Fan Z, Zhang Y, Xu J, Wang H, Feng L (2001) *Polymer* 42:5559
55. Xu J, Feng L, Yang S, Wu Y (1997) *Polymer* 38:4381
56. Sun Z, Yu F, Qi Y (1991) *Polymer* 32:1059

57. Feng Y, Hay JN (1998) *Polymer* 39:6723
58. Randall JC (1989) *JMS-Rev Macromol Chem Phys* C29:201
59. Tosi C, Ciampelli F (1973) *Adv Polym Sci* 12:87
60. Baker BB, Bonesteel JK, Keating MY (1990) *Thermochim Acta* 166:53
61. Xu J, Fu Z, Fan Z, Feng L (2002) *Eur Polym J* 38:1739
62. Zacur R, Goizueta G, Capiati N (1999) *Polym Eng Sci* 39:921
63. Ray GJ, Johnson PE, Knox JR (1977) *Macromolecules* 10:773
64. Randall JC (1978) *Macromolecules* 11:33
65. Kanezaki T, Kume K, Sato K, Asakura T (1993) *Polymer* 34:3129
66. Zacur R, Goizueta G, Capiati N (2000) *Polym Eng Sci* 40:1921
67. Nakatani H, Manabe N, Yokota Y, Minami H, Suzuki S, Yamaguchi F, Terano M (2007) *Polym Int* 56:1152
68. Kakugo M, Miyatake T, Mizunuma K, Kawai Y (1988) *Macromolecules* 21:2309
69. Pasch H, Trathnigg B (2013) *Multidimensional HPLC of polymers*. Springer, Berlin
70. Verstrate G, Cozewith C, West RK, Davis WM, Capone GA (1999) *Macromolecules* 32:3837
71. Ozzetti RA, De Oliveira Filho AP, Schuchardt U, Mandelli DJ (2000) *Appl Polym Sci* 85:734
72. Albrecht A, Heinz LC, Lilje D, Pasch H (2007) *Macromol Symp* 257:46
73. Bly RM, Kiener PE, Fries BA (1966) *Anal Chem* 38:217
74. Luongo JJP (1960) *Appl Polym Sci* 3:302
75. Andreassen E (1999) Infrared and Raman spectroscopy of polypropylene. In: Karger-Kocsis J (ed) *Polypropylene: an A-Z reference*. Kluwer, Dordrecht, p 320
76. Painter PC, Watzek M, Koenig JL (1977) *Polymer* 18:1169
77. Monasse B, Haudin JM (1995) Molecular structure of polypropylene homo- and copolymers. In: Karger-Kocsis J (ed) *Polypropylene: structure, blends and composites*. Chapman & Hall, London
78. Quynn RG, Riley JL, Young DA, Noether HDJ (1959) *Appl Polym Sci* 2:166
79. Stein RS, Sutherland GBBM (1953) *J Chem Phys* 21:370
80. Tobin MC, Carrano MJJ (1957) *Polym Sci* 24:93
81. Drushel HV, Iddings FA (1963) *Anal Chem* 35:28
82. Snyder RG, Maroncelli M, Strauss HL, Hallmark VM (1986) *J Phys Chem* 90:5623
83. de Goede E, Mallon P, Pasch H (2012) *Macromol Mater Eng* 297:26
84. Struik LCE (1987) *Polymer* 28:1521
85. Halim Hamid S (2000) *Handbook of polymer degradation*. Marcel Dekker, New York, NY
86. Michaeli W, Bittner M (1992) In: Menges G, Michaeli W, Bittner M (eds) *Recycling von Kunststoffen*. Carl Hanser, München
87. Kroschwitz J (1986) *Encycl Polym Sci*. Wiley, New York, NY
88. Bolland JL, Gee G (1946) *Trans Faraday Soc* 42:236
89. Bolland JL, Gee G (1946) *Trans Faraday Soc* 44:669
90. Gugumus G (1995) *Polym Degrad Stab* 49:28
91. Niki E, Dekker C, Mayo FR (1973) *J Polym Sci Part A Polym Chem* 11:2813
92. Adams JH (1970) *J Polym Sci Part A-1* 8:1077
93. Adams JH, Goodrich JE (1970) *J Polym Sci Part A-1* 8:1269
94. Lacoste J, Vaillant D, Carlsson DJ (1993) *J Polym Sci Part A Polym Chem* 31:715
95. Gijsman P, Kroon M, van Oorschot M (1996) *Polym Degrad Stab* 51:8
96. Lacoste J, Carlsson DJ (1992) *J Polym Sci Part A Polym Chem* 30:493
97. de Goede S, Brüll R, Pasch H, Marshall N (2003) *Macromol Symp* 193:35
98. de Goede S, Brüll R, Pasch H, Marshall N (2004) *e-polymers* no. 012
99. de Goede E, Mallon P, Pasch H (2011) *Macromol Mater Eng* 296:1018
100. Pasch H, de Goede E, Mallon P (2012) *Macromol Symp* 312:174
101. Monrabal B (1991) Crystallization analysis fractionation. US Patent 5,222,390
102. Soares JBP, Anantawaraskul S (2005) *J Polym Sci Part B Polym Phys* 43:1557
103. Monrabal B, Blanco J, Nieto J, Soares JBP (1999) *J Polym Sci Part A Polym Chem* 37:89
104. Pasch H, Brüll R, Wahner U, Monrabal B (2000) *Macromol Mater Eng* 279:46

105. Wild L (1993) *Trends Polym Sci* 1:50
106. Karoglanian SA, Harrison IR (1996) *Polym Eng Sci* 36:731
107. Soares JBP, Hamiliac AE (1995) *Polymer* 36:1639
108. Mara JJ, Menard KP (1994) *Acta Polym* 45:378
109. Joskowicz PL, Munoz A, Barrera J, Mueller AJ (1995) *Macromol Chem Phys* 196:385
110. Brüll R, Pasch H, Raubenheimer HG, Sanderson RD, van Reenen AJ, Wahner UM (2001) *Macromol Chem Phys* 202:1281
111. Alamo RG, Mandelkern L (1994) *Thermochim Acta* 238:155
112. Arnold M, Henschke O, Knorr J (1996) *Macromol Chem Phys* 197:563
113. Monrabal B, del Hierro P (2011) *Anal Bioanal Chem* 399:1557
114. Monrabal B, Sancho-Tello J, Mayo N, Romero L (2007) *Macromol Symp* 257:71

Advanced Separation Techniques for Polyolefins

Pasch, H.; Malik, M.I.

2014, XII, 179 p. 121 illus., 44 illus. in color., Hardcover

ISBN: 978-3-319-08631-6